7834 Revision 1

Keplerite, $Ca_9(Ca_{0.5}\square_{0.5})Mg(PO_4)_7$, a new meteoritic and terrestrial phosphate isomorphous with merrillite, $Ca_9NaMg(PO_4)_7$

Sergey N. Britvin[1,2,*], Irina O. Galuskina[3], Natalia S. Vlasenko[4], Oleg S. Vereshchagin[1], Vladimir N. Bocharov[4], Maria G. Krzhizhanovskaya[1], Vladimir V. Shilovskikh[4,5], Evgeny V. Galuskin[3], Yevgeny Vapnik[6], and Edita V. Obolonskaya[7]

[1] Institue of Earth Sciences, St. Petersburg State University, Universitetskaya Nab. 7/9, 199034 St. Petersburg, Russia

[2] Kola Science Center, Russian Academy of Sciences, Fersman Str. 14, 184209 Apatity, Russia

[3] Faculty of Natural Sciences, Institute of Earth Sciences, University of Silesia, Bedzińska 60, 41–200 Sosnowiec, Poland

[4] Centre for Geo-Environmental Research and Modelling, St. Petersburg State University, Ulyanovskaya str. 1, 198504 St. Petersburg, Russia

[5] Institute of Mineralogy, Urals Branch of Russian Academy of Science, Miass 456317, Russia

[6] Department of Geological and Environmental Sciences, Ben-Gurion University of the Negev, POB 653, Beer-Sheva 84105, Israel

[7] The Mining Museum, Saint Petersburg Mining University, 2, 21st Line, 199106 St. Petersburg, Russia

*Corresponding author. E-mail: sergei.britvin@spbu.ru

Abstract

Keplerite is a new mineral, the Ca-dominant counterpart of the most abundant meteoritic phosphate, merrillite. The isomorphous series merrillite–keplerite, $Ca_9NaMg(PO_4)_7$ –$Ca_9(Ca_{0.5}\square_{0.5})Mg(PO_4)_7$ represents the main reservoir of phosphate phosphorus in the Solar System. Both minerals are related by the heterovalent substitution at the *B*-site of the crystal structure: $2Na^+$ (merrillite) → Ca^{2+} + □ (keplerite). The near-end-member keplerite of meteoritic origin occurs in the main-group pallasites and angrites. The detailed description of the mineral is made based on the Na-free type material from the Marjalahti meteorite (the main group pallasite). Terrestrial keplerite was discovered in the pyrometamorphic rocks of the Hatrurim Basin in the northern part of Negev desert, Israel. Keplerite grains in Marjalahti have an ovoidal to cloudy shape and reach 50 μm in size. The mineral is colorless, transparent with a vitreous luster. Cleavage was not observed. In transmitted light, keplerite is colorless and non-pleochroic. Uniaxial (−), ω 1.622(1), ε 1.619(1). Chemical composition (electron microprobe, wt.%): CaO 48.84; MgO 3.90; FeO 1.33; P_2O_5 46.34, total 100.34. The empirical formula (O = 28 *apfu*) is: $Ca_{9.00}(Ca_{0.33}Fe^{2+}_{0.20}\square_{0.47})_{1.00}Mg_{1.04}P_{6.97}O_{28}$. The ideal formula is $Ca_9(Ca_{0.5}\square_{0.5})Mg(PO_4)_7$. Keplerite is trigonal, space group *R*3*c*, unit-cell parameters refined from single-crystal data are: *a* 10.3330(4), *c* 37.0668(24) Å, *V* 3427.4(3) Å^3, *Z* = 6. The calculated density is 3.122 g cm^{-3}. The crystal structure has been solved and refined to R_1 = 0.039 based on 1577 unique observed reflections [$I > 2\sigma(I)$]. A characteristic structural feature of keplerite is a partial (half-vacant) occupancy of the sixfold-coordinated *B*-site (denoted as CaIIA in the earlier works). The disorder caused by this cation vacancy is the most likely reason for the visually resolved splitting of the ν_1 (symmetric stretching) (PO_4) vibration mode in the Raman spectrum of keplerite. The mineral is an indicator of high-temperature environments characterized by extreme depletion of Na. The association of keplerite with "*REE*-merrillite" and stanfieldite evidences for the similarity of temperature conditions occurred in the Mottled Zone to those

expected during formation of pallasite meteorites and Lunar rocks. Because of cosmochemical significance of merrillite-keplerite series and by analogy to plagioclases, the Na-number measure, 100×Na/(Na+Ca) (*apfu*), is herein proposed for the characterization of solid solutions between merrillite and keplerite. The merrillite end-member, $Ca_9NaMg(PO_4)_7$, has the Na-number = 10 whereas keplerite, $Ca_9(Ca_{0.5}\square_{0.5})Mg(PO_4)_7$, has Na-number = 0. Keplerite (IMA 2019-108) is named in honor of Johannes Kepler (1571–1630), a prominent German naturalist, for his contributions to astronomy and crystallography.

Keywords: keplerite, merrillite, whitlockite, phosphate, meteorite, pallasite, angrite, pyrometamorphism

This is the peer-reviewed, final accepted version for American Mineralogist, published by the Mineralogical Society of America.
The published version is subject to change. Cite as Authors (Year) Title. American Mineralogist, in press.
DOI: https://doi.org/10.2138/am-2021-7834. http://www.minsocam.org/

Introduction

The whitlockite group incorporates 8 natural phosphates whose general chemical formula can be expressed as $A_9BM(PO_3X)_4(PO_4)_3$, where the species-defining constituents A = Ca or Sr; B = Na, Ca or □ (vacancy); M = Mg, Fe^{2+} or Mn^{2+}; and X is either O or OH (Table 1). Among these minerals, two species are of particular importance in biochemistry and planetary science. The water-containing whitlockite, $Ca_9Mg(PO_3OH)(PO_4)_6$, is a very rare terrestrial phosphate (Frondel 1941; 1943) but a common constituent of all vertebrates' bone tissues (Wang and Nancollas 2008). The anhydrous species, merrillite, $Ca_9NaMg(PO_4)_7$, the first discovered whitlockite-group mineral (Merrill 1915), is the most abundant meteoritic phosphate, a dominant carrier of phosphate phosphorus in the cosmic matter. Merrillite is a common accessory phase of ordinary chondrites (Fuchs 1962; Van Schmus and Ribbe 1969; Jones et al. 2014, 2016; Lewis and Jones 2016); it occurs in carbonaceous chondrites, many groups of achondrites, stony-iron and iron meteorites (Buseck and Holdsworth 1977; Ward et al. 2017) in Lunar rocks and Martian meteorites (Jolliff et al. 2006; Shearer et al. 2015). It is considered to be the primary phosphate phase formed during protoplanetary nebula condensation (Pasek 2015). Merrillite forms a continuous series of solid solutions with its Fe^{2+}-dominant analogue, ferromerrillite, $Ca_9NaFe(PO_4)_7$ – a phosphate typical of Martian shergottites (Britvin et al. 2016). Terrestrial merrillite was discovered in mantle xenoliths from Siberia, Russia (Ionov et al. 2006), and was recently encountered in phosphate assemblages of pyrometamorphic rocks belonging to the Hatrurim Formation, Israel (Galuskina et al. 2016). Merrillite has three notable chemical features. First, this is a water-free mineral, in contrast to a majority of terrestrial whitlockite-group members which bear water as a constituent of hydrogen phosphate groups (Table 1). Second, merrillite is devoid of F and Cl. Last, the mineral contains an appreciable amount of Na. The two latter features highlight the differences between merrillite and another abundant meteoritic phosphate – apatite (McCubbin and Jones 2015; Ward et al. 2017).

Merrillite is an important reservoir for meteoritic Na. The mineral tends to accumulate even the traces of Na available in the mineral system (e.g., Buseck and Holdsworth 1977). However, upon complete lack of this element in the environment, the only way to maintain the charge balance and structure of merrillite is to compensate Na by other elements. The prime candidates for such a replacement are Ca and *REE* (e.g., Jolliff et al. 2006; Hughes et al. 2006).

There are two meteorite groups whose members are extremely depleted in Na – these are the pallasites and angrites. Pallasites are the stony-iron meteorites considered as products of fractional melting of chondrite parent body (Boesenberg et al. 2012). Angrites have basaltic composition and textures, and they are the most alkali-depleted basalts in the Solar System (Keil 2012). It is thus not surprising that the first finding of Ca-dominant analogue of merrillite was confined to the angrite meteorite, Angra dos Reis (Dowty 1977). In the same year, Buseck and Holdsworth (1977) have published a detailed report on phosphate mineral assemblages in pallasites, where they have identified the similar Na-depleted Ca-phosphate. At that time, meteoritic merrillite was not definitely recognized as an analogue of whitlockite: the crystal structure of natural merrillite, $Ca_9NaMg(PO_4)_6$, was determined much later (Xie et al. 2015; Britvin et al. 2016). The absence of knowledge regarding the relationships between merrillite and whitlockite has led to ambiguities in naming of these minerals (see Adcock et al. 2014). Because of that, both Dowty (1977) and Buseck with Holdsworth (1977) ascribed the reported mineral to whitlockite, whose formula was at that time accepted as $Ca_3(PO_4)_2$, by analogy to synthetic β-$Ca_3(PO_4)_2$ (Frondel 1941).

Although the mineral from Angra dos Reis (Dowty 1977) is essentially enriched in Ca, it still contains noticeable amount of Na (Keil et al. 1976) (Table 2). However, a survey of analyses reported by Buseck and Holdsworth (1977) reveals "whitlockite" having considerably lower Na_2O content, down to the Na-free phosphate occurring in the Marjalahti and Ahumada pallasites (Table 2). We have determined the crystal structure of the latter mineral and found that it represents the Na-free counterpart of merrillite previously known as a synthetic dehydrogenation product of

This is the peer-reviewed, final accepted version for American Mineralogist, published by the Mineralogical Society of America.
The published version is subject to change. Cite as Authors (Year) Title. American Mineralogist, in press.
DOI: https://doi.org/10.2138/am-2021-7834. http://www.minsocam.org/

whitlockite (Hughes et al. 2008; Adcock et al. 2014). Consequently, this is a new mineral species distinct from both merrillite and whitlockite (Table 1). In the course of an ongoing research of the unusual pyrometamorphic complex, the Hatrurim Formation (the Mottled Zone) in the Southern Levant, the same mineral has been confirmed in the Hatrurim Basin, Negev desert, Israel. Therefore, this Na-depleted analogue of merrillite is currently recognized as both meteoritic and terrestrial species. The new mineral was named keplerite, in honor to Johannes Kepler (1571–1630), a prominent German scientist, for his contributions to astronomy and crystallography (e.g., Kepler 1611). Both the mineral and the name have been approved by the Commission on New Minerals, Nomenclature and Classification of the International Mineralogical Association (IMA 2019-108). The holotype specimen of keplerite from the Marjalahti pallasite is deposited in the collections of the Mining Museum, Saint Petersburg Mining University, St. Petersburg, Russia, catalogue number MM74/2-1.

Materials and Methods

The specimens. The pieces of the Marjalahti and the Brahin pallasites (MM74/2 and MM65/2, respectively) were kindly provided for this study by the curators of the Mining Museum, Saint Petersburg Mining University. The chip of the Los Angeles shergottite was obtained from Sergey Vasiliev (sv-meteorites.com). The specimens containing terrestrial keplerite were collected by I.O.G., E.V.G. and Ye.V. during the field trips. ***Electron microprobe analyses (EMPA) and SEM study*** of meteoritic keplerite and associated minerals were carried out on the polished carbon-coated sections by means of a Hitachi S-3400N SEM with an attached INCA WAVE 500 WDX spectrometer (20 kV, 10 nA), using the following standards and lines: chlorapatite (Ca*K*α, P*K*α); diopside (Mg*K*α) and hematite (Fe*K*α). A complete set of chemical analyses of holotype keplerite from the Marjalahti meteorite is given in Supplementary Table S1. Chemical composition of terrestrial keplerite and associated minerals was studied by means of a CAMECA SX100 WDX

This is the peer-reviewed, final accepted version for American Mineralogist, published by the Mineralogical Society of America.
The published version is subject to change. Cite as Authors (Year) Title. American Mineralogist, in press.
DOI: https://doi.org/10.2138/am-2021-7834. http://www.minsocam.org/

analyzer (15 kV, 20 nA) using the following standards and lines: fluorapatite (P*K*α, F*K*α); diopside (Mg*K*α, Ca*K*α, Si*K*α); orthoclase (Al*K*α, K*K*α); hematite (Fe*K*α); rhodochrosite (Mn*K*α); albite (Na*K*α); baryte (Ba*L*α, S*K*α); celestine (Sr*L*α); V_2O_5 (V*K*α); YPO_4 (Y*L*α); La-glass-Geochr (La*L*α); CeP_5O_{11} (Ce*L*α); SmP_5O_{11} (Sm*L*β); $NdGeO_3$ (Nd*L*β); Pr-glass-Geochr (Pr*L*β). ***X-ray single-crystal study*** of the type keplerite crystal was performed based on the data collected with a Bruker Kappa APEX DUO diffractometer equipped with a microfocus Mo*K*α-radiation source and 1024K APEXII CCD detector. Data collection and unit-cell refinement were performed using a built-in Bruker APEX2 program package, whereas integration procedures were carried out with a CrysAlisPro software (Rigaku Oxford Diffraction 2018). Crystal structure solution and refinement was carried out with the HKL dataset truncated at 2Θ = 54°, using a *SHELX*-2018 program suite incorporated into the Olex2 operational environment (Sheldrick 2015; Dolomanov et al. 2009). The complete set of data collection and structure refinement details can be retrieved from the Crystallographic Information File (CIF) attached to the Supplementary Materials. A brief summary of data collection and refinement parameters is given in Supplementary Table S2. ***Powder X-ray diffraction.*** The powder X-ray diffraction pattern of holotype keplerite was calculated on the basis of structural data (Supplementary Table S3). ***Optical study*** was performed using a Leica DM 4500P polarizing microscope and a standard set of immersion liquids. The metal sections intended for the study in reflection light were preliminary etched with nital solution (2 parts of 65% HNO_3 per 98 parts of ethanol). ***Raman spectra*** of meteoritic (holotype) keplerite were recorded with a Horiba Jobin-Yvon LabRam HR800 instrument equipped with an Ar-ion laser (λ = 514 nm), using an Olympus BX41 microscope through the 50× confocal objective. The spectral resolution was set to 2 cm^{-1}, acquisition time was 30 s and the each dataset was averaged from 20 scans. The spectrometer was preliminary calibrated using a 520.7 cm^{-1} line of a silicon standard. Raman spectra of terrestrial keplerite were recorded on a WITec alpha 300R Confocal Raman Microscope equipped with an air-cooled solid-state laser (532 nm) and 100× confocal objective. Integration times of 5 s with an

accumulation of 20-30 scans and a resolution 2 cm^{-1} were chosen. The monochromator was calibrated using the Raman scattering line of a silicon plate (520.7 cm^{-1}).

Results

Occurrence, appearance and properties

The Marjalahti pallasite (type locality). A few fragments of the ~45 kg Marjalahti mass were harvested on June 01, 1902 shortly after the meteorite fall that hit the granite outcrop at the Marjalahti bay, northern coast of the Lake Ladoga, Karelia, Russia. Being one of four witnessed pallasite falls (Grady 2000), Marjalahti was not affected to weathering. Like other main-group pallasites, the meteorite consists of cm-sized olivine crystals embedded into the α-(Fe,Ni) (kamacite) matrix. The α-(Fe,Ni) metal of the studied Marjalahti section contains 5.7 wt.% Ni and 0.85 wt.% Co; it is penetrated by a dense net of Neumann bands – the traces of shock-induced deformation twins revealed by nital etching (Figure 1) (e.g., Uhlig 1955). Subordinate mineral phases of Marjalahti include chromite, troilite, schreibersite, nickelphosphide, tetrataenite, and trace amounts of nazarovite, $Ni_{12}P_5$ (IMA 2019-013). The Marjalahti phosphate, being recognized as merrillite, was a subject of research aimed at determination of its fission track age (e.g., Pellas et al. 1983). However, there are no analytical data evidencing for the occurrence of genuine merrilite, $Ca_9NaMg(PO_4)_7$ in this meteorite.

Keplerite in Marjalahti is confined to the specific troilite-orthopyroxene vermicular intergrowths (symplectites) developed along the contacts between olivine and Fe-Ni metal (Figure 2). The assignment of pyroxene to the orhorhombic enstatite was made by the use of a single-crystal XRD analysis. Troilite in symplectites and in adjacent grains (Figure 2a,b) has a perfect FeS stoichiometry and does not contain detectable Cr, V or Ti impurities. It is noteworthy that troilite inclusions on contact with symplectites have a pronounced outer rims composed of microgranular porous troilite. Keplerite occurs as chains of ovoidal to cloud-like inclusions in both olivine and

185 orthopyrohene, at the peripheral zone of symplectites, immediately at the borderline with (Fe,Ni)
186 metal. The biggest grain encountered was ~40 μm in length. Keplerite is colorless, transparent with
187 a vitreous lustre and shows no cleavage. It is non-fluorescent under long- and short-UV light.
188 Examination in the immersion liquids in transmitted light showed the mineral is colorless and non-
189 pleochroic. It is uniaxial, (−), ω 1.622(1), ε 1.619(1). The Gladstone-Dale compatibility index
190 (Mandarino 1981) is –0.010 (superior). The density calculated based on the empirical formula and
191 the unit-cell volume refined from single-crystal X-ray diffraction data is 3.122 g cm^{-3}.

192 ***The Hatrurim Basin.*** Being the largest complex of pyrometamorphic rocks in Israel, the
193 Hatrurim Basin occupies an area of ~50 km^2 a few kilometers to the west of the southern subbasin of
194 the Dead Sea. Hatrurim Basin belongs to a pyrometamorphic suite known as the Hatrurim
195 Formation or the Mottled Zone (e.g., Gross 1977; Burg et al. 1999; Vapnik et al. 2007; Geller et al.
196 2012; Novikov et al. 2013) . The diverse mineralogy of the Hatrurim Formation gathers Earth's
197 exotic and often genetically incompatible mineral assemblages produced by superposition of several
198 processes: (1) Pyrometamorphism at the temperature reaching 1400 °C, that has led to the
199 calcination and fusion of sedimentary strata and was accompanied by the formation of paralavas and
200 high-temperature alteration of the early "clinker" mineral associations; (2) post-metamorphic low-
201 temperature hydrothermal activity and (3) supergene alteration of high-temperature assemblages
202 (Gross 1977; Galuskina et al. 2014; Britvin et al. 2015; Galuskin et al. 2016; Sokol et al. 2019;
203 Khoury 2020). Keplerite is confined to the rocks belonging to the pyrometamorphic stage. The
204 mineral was identified in the brecciated, altered pyroxene paralava (fused sediments) outcropped on
205 the slope of a hill in the Negev Desert near the town of Arad (31° 13′ 58″ N; 35° 16′ 2″ E). (Figure
206 3). The paralava forms an irregular rounded field of ~20 m across, within the area occupied by the
207 grey and red spurrite marbles. The marbles in the vicinity of the reported locality are known for the
208 diversity of exotic minerals, such as ariegilatite, stracherite, and aravaite (Galuskin et al. 2018a,b;
209 Krüger et al. 2018). Large blocks of brecciated paralava are color-zoned – from brick-red to grey in

the central parts to olive-green at the periphery. The interiors of the blocks are filled with the paralava fragments of two types, distinguished by the composition and color. The first type is comprised by the fine-grained grey angular chunks (Figure 4a) composed of diopside [mean composition $(Ca_{0.94}Na_{0.06})(Mg_{0.82}Fe^{3+}_{0.11}Al_{0.07})(Si_{1.88}Al_{0.12})O_6$], subordinate wollastonite, andradite and rare anorthite. The red rims circumfering the grey fragments are colored by finely dispersed hematite (Figure 4b). The rock fragments of the second type have a yellow-green color (Figure 4a); they fill up the interstices between the grey fragments. The yellow-green rocks consist of the fine grains of diopside-esseneite pyroxene [mean composition $Ca(Mg_{0.7}Fe^{3+}_{0.2}Al_{0.1})(Si_{1.7}Al_{0.3})O_6$], wollastonite and fluorapatite which are dispersed within the matrix of secondary zeolites, Ca-hydrosilicates, hydrogarnets and calcite. The diopside-esseneite grains are commonly outlined by the thin zones of aegirine [mean composition $(Na_{0.59}Ca_{0.41})(Fe^{3+}_{0.57}Mg_{0.31}Fe^{2+}_{0.10}Al_{0.01})Si_2O_6$]. The rock fragments of both types are cemented and penetrated by a white-colored suite of the late minerals, including baryte, calcite, zeolites, tacharanite, afwillite and tobermorite-group silicates (Figure 4a b). The hematite nodules reaching several cm in size are the specific feature of the reported paralava. Besides of dominating hematite, the nodules contain magnesioferrite, maghemite, ilmenite, pseudobrookite, hibonite, dorrite, and kahlenbergite, $KAlFe_{10}O_{17}$ (Krüger et al. 2019). The minerals related to the join merrillite–keplerite occur as the aggregates up to 0.2 mm in size scattered within the fine-grained grey paralava; they are often intergrown with fluorapatite and likely replace the latter (Figure 4c-e, Table 3). Monazite and xenotime inclusions are observed in those fluorapatite crystals which are not intergrown with keplerite (Figure 4f). A merrillite-like mineral with anomalously high *REE* content, $(Ca,REE)Mg(PO_4)_7$, and stanfieldite are rarely encountered in the same association (Figure 4e, Table 3). This is the first terrestrial occurrence of *REE*-bearing merrillite-group mineral and stanfieldite, both previously known only in the Lunar rocks and meteorites (Jolliff et al. 2006; Britvin et al. 2020).

Chemical composition

The summary of the chemical data on meteoritic keplerite is provided in Table 2; the data on terrestrial keplerite are given in Table 3. The characteristic feature of terrestrial keplerite, distinguishing it from the meteoritic one, is the presence of *REE* and the low iron content. One can see that the majority of keplerite analyses, including those for the mineral from Angra dos Reis (Keil et al. 1976; Dowty 1977) show noticeable contents of Na and hence represent the intermediate members of solid solutions between keplerite and merrillite. Keplerite from Marjalahti (and Ahumada) is unique in this respect as it does not contain Na. Besides, there are two chemical features of the Marjalahti mineral which are directly related to its origin and crystal structure. The orthopyroxene ($En_{0.88}Fs_{0.12}$) in keplerite-containing symplectites (Figure 2) and adjacent olivine ($Fo_{0.88}Fa_{0.12}$) have the same Mg-number [100×Mg/(Mg+Fe)] equal to 88 (Supplementary Table S4). The Mg-number of keplerite is 83 – the mineral is obviously enriched in Fe relative to both coexisting silicates. The empirical formula of the type Marjalahti keplerite, calculated on the basis of 28 oxygen atoms per formula unit (*apfu*), is $Ca_{9.00}(Ca_{0.33}Fe^{2+}_{0.20}\square_{0.47})_{1.00}Mg_{1.04}P_{6.97}O_{28.00}$. Therefore, the sum of *M*-site cations, i.e., (Mg+Fe) is equal to 1.24 *apfu* that is considerably higher than the unity dictated by the ideal keplerite stoichiometry, $Ca_9(Ca_{0.5}\square_{0.5})Mg(PO_4)_7$. The substantial excess of (Mg+Fe) was previously reported for the mineral from Marjalahti and for keplerite of the same, "symplectic" origin from the Ahumada pallasite (Table 2) (Buseck and Holdsworth 1977). At the same time, keplerite and merrillite of non-symplectic origin and terrestrial mineral do not exhibit (Mg+Fe) excess. Therefore, the observed "extra" contents of octahedral cations in keplerite from symplectites are not an artifact and thus require explanation which is given below.

Crystal structure

The basic features of keplerite structure are the same as of other whitlockite-group minerals whose general structural formula can be expressed as $[A(1)_3\ A(2)_3\ A(3)_3]\ B\ M\ [P(1)\ P(2)_3\ P(3)_3]\ O_{24}\ X_4$, leading to a chemical formula $A_9BM(PO_3X)_4(PO_4)_3$ (Table 1). The whitlockite-type framework consists of an arrangement of $[PO_4]$ tetrahedra and cation-centered polyhedra $[AO_8]$, $[BO_6]$ and $[MO_6]$ linked via the common corners and edges, forming a series of rods propagated along the *c*-axis (Gopal and Calvo 1972; Moore 1973). The arrangement of species-defining $[BO_6]$ and $[MO_6]$ polyhedra is shown in Figure 5. The $[MO_6]$ unit in the whitlockite structure type is a slightly distorted octahedron readily adopting Mg^{2+}, Fe^{2+} or Mn^{2+} (Table 1). There are no references evident for the possibility of vacancies at the *M*-site. The free refinement of the *M*-site population in the type keplerite from the Marjalahti pallasite shows that this position is occupied solely by Mg^{2+}, consistent with the equality of *M*–O bond lengths in Marjalahti keplerite and classic merrillite having near-zero Fe contents (Table 4). In contrast, the *M*–O bond lengths in the mineral from Angra dos Reis (Dowty 1977) are noticeably longer, in accordance with the higher Fe^{2+} population at the *M*-site (Table 4). Therefore, considering that the total (Mg+Fe) content in type keplerite substantially exceeds the unity (in *apfu*) (Table 2), there must be another structural position capable of accommodating the observed excess of Fe^{2+}.

The $[BO_6]$ polyhedron (denoted as the CaIIA site in the earlier works (e.g., Calvo and Gopal 1975; Dowty 1977) has a shape of apex-truncated trigonal pyramid slightly twisted about the *c*-axis (Figure 5, 6a). In the anhydrous members of whitlockite group, the *B*-site is partially or fully occupied by either Ca^{2+} or Na^{+} and shares a common face with the $[P(1)O_4]$ tetrahedron (Figure 6a). In the hydrogen-bearing members, the $[P(1)O_4]$ tetrahedron is inverted along the *c*-axis, being tied up with three $[P(2)O_4]$ tetrahedra via the hydrogen atom and the system of hydrogen bonds (Figure 6b) (e.g., Belik et al. 2003). Consequently, the *B*-site in the hydrogen-bearing whitlockite-group minerals is not vacant, but it is occupied by the P–O pair of $[P(1')O_4]$ and the H atom(s) (Figure 6b).

Consequently, the location of [$P(1)O_4$] tetrahedron relative to the truncated apex of the *B*-site allows structural distinguishing between the anhydrous and hydrous members of the whitlockite group (Table 1). In particular, the attachment of [PO_4] tetrahedron to the truncated apex of the *B*-site (Figure 6a) unambiguously evidences that keplerite from Marjalahti does not contain hydrogen. The freely refined site scattering factor of the *B*-site in keplerite is equal to 9.90 electron units, that well corresponds to the mean atomic number of 11.80 derived from EMPA results (Table 2 and 4). The latter give the total Ca content of 9.33 *apfu* (Table 2), that, after subtraction of 9 Ca atoms residing in the [AO_8] polyhedra, leaves 0.33 Ca atoms at the *B*-site. It should be noted, however, that due to the methodology of chemical calculations, the *B*-site population is a residual value which accumulates all the analytical errors emerging in the course of EMPA (e.g., Shearer et al. 2015). The standard uncertainty of Ca determinations by electron microprobe is in the order of ~1-1.3 relative % (e.g., Jolliff et al. 2006), that corresponds to 0.05-0.06 Ca *apfu* and thus figures out 0.33(3) Ca *apfu* residing at the *B*-site. Therefore, there is still enough vacant space at the *B*-site (0.67 *apfu*) which can accomodate other cations. Consequently, the observed excess of (Fe+Mg) in the Marjalahti mineral (Buseck and Holdsworth 1977 and our data, Table 2) might indicate that Fe^{2+} in holotype keplerite incorporates into the *B*-site. This suggestion agrees well with the six-fold coordination of the *B*-site, contrary to the eight-fold one of [AO_8] polyhedra, and supported by previous reports on the same type of *B*-site substitutions in whitlockite-related phosphates (Schroeder et al. 1977; Britvin et al. 1991; Belik et al. 2003). The final structural refinement carried out assuming a fixed ($Ca_{0.33}Fe_{0.20}$) *B*-site population has perfectly converged (see the attached CIF file), confirming the correctness of the chemical formula determined from electron microprobe data.

Raman spectroscopy

The Raman spectrum of the holotype keplerite from the Marjalahti pallasite is shown in Figure 7 in comparison with the spectra of merrillite and ferromerrillite whose crystal structures were reported

309 previously (Britvin et al. 2016). The absence of the band at 923 cm^{-1} evidences for the lack of
310 hydrogen phosphate groups (Jolliff et al. 1996), in accordance with the results of the structure
311 refinement. All three minerals exhibit the similar sets of Raman bands between 400 and 1080 cm^{-1}
312 related to vibration modes of $[PO_4]$ tetrahedra (de Aza et al. 1997; Kovyazina et al. 2004; Jolliff et
313 al. 2006) (Table 5). However, the strongest stretching vibration modes at 950-970 cm^{-1} in the
314 spectrum of keplerite have a complex structure which is not observed in the spectra of merrillite and
315 ferromerrillite (Figure 7). The profile deconvolution (Lorenz shape approximation) gives in total 6
316 bands with the following fitted parameters [wavenumber (relative intensity, FWHM, cm^{-1})]: 950
317 (31, 6.7); 954 (35, 6.2); 958 (12. 7.6); 962 (10, 6.3); 968 (19, 6.3); and 971 (59, 5.3). The bands at
318 954 and 971 cm^{-1} coincide with the commonly observed ν_1 modes in the spectra of merrillite (e.g.,
319 Jolliff et al. 2006; Xie et al. 2015). However, to the best of our knowledge, the visually resolved
320 shoulders at 950 and 958 cm^{-1} were not reported previously. These bands were observed in the
321 Raman spectra of five different keplerite grains and thus are neither the artifacts nor the phenomena
322 related to the crystal orientation. The most likely explanation for their emergence are the local
323 distortions in $[P(1)O_4]$ and $[P(2)O_4]$ tetrahedra adjoining the statistically half-occupied *B*-site
324 (Figure 6). The Raman spectra of terrestrial keplerite (Supplementary Figure S1) are close to the
325 spectra of minerals of the merrillite subgroup (Jolliff et al. 2006; Xie et al. 2015), bearing a
326 characteristic duplet 956-958 and 973-974 cm^{-1}.
327

328 **Discussion**

329 **The origin of keplerite**

330 The formation conditions of keplerite, $Ca_9(Ca_{0.5}\square_{0.5})Mg(PO_4)_7$ require the complete lack of Na and
331 water in a mineral system. The presence of Na facilitates crystallization of intermediate merrillite-
332 keplerite phases, whereas aqueous medium can result in the emergence of whitlockite,

333 $Ca_9Mg(PO_3OH)(PO_4)_6$. Accumulation of even traces of Na in the residual melts of pallasite
334 meteorites leads to the emergence of merrillite – the sole Na-bearing phase in pallasites (Buseck and
335 Holdsworth 1977). However, keplerite was discovered in another type of pallasite assemblages – in
336 the orthopyroxene-troilite symplectites (Figure 1) (Buseck 1977; Buseck and Holdsworth 1977).
337 The two-phase composition and vermicular textures of these intergrowths are the same as of
338 symplectites reported in acapulcoites (El Goresy et al. 2005; Folco et al. 2006), howardites (Patzer
339 and McSween 2012) and brachinites (Goodrich et al. 2017). Although the above authors agree that
340 the symplectites represent the quenched sulfide-silicate melts, the nature of an event(s) responsible
341 for their formation is a matter of debates. Concerning the Marjalahti symplectites described herein,
342 the apparent evidence is that they were formed prior to the shock event caused the emergence of the
343 Neumann bands (Figure 1 and 2), otherwise the latter would be annealed during the heating process.
344 However, the Neumann bands could be produced at the latest stage, upon the collision of the
345 meteorite with the granite outcrop, as the projectile velocity was obviously sufficient for that (e.g.,
346 Uhlig 1955; Beck 2011). An interesting insight can be inferred from the results of a fission-track
347 dating of the so-called “whitlockite” from Marjalahti (Pellas et al. 1983; Bondar and Perelygin
348 2005). Because neither Buseck and Holdsworth (1977) nor our study did reveal the occurrence of
349 merrillite in Marjalahti, one can suppose that the Na-free “whitlockite” used for the fission-track
350 analysis was in fact represented by keplerite. As a result, keplerite and symplectites could have an
351 age of ~4.3 Ga (Bondar and Perelygin 2005) and hence be directly related to the early crystallization
352 history of Marjalahti. In that case, one can rule out the hypothesis of atmospheric ablation-induced
353 origin of Marjalahti symplectites, like that proposed for the similar Acapulco assemblages (El
354 Goresy et al. 2005). It is important that the Mg-number of orthopyroxene in the symplectites from
355 the Marjalahti pallasite is the same as of adjacent olivine crystals not affected to melting (Mg# =
356 88). Therefore, it is unlikely that the parent melts of the Marjalahti symplectites were subjected to
357 redox differentiation (e.g., Righter et al. 1990), and the system was apparently the chemically closed

and equilibrated one. The microgranular texture of troilite adjacent to symplectites inspires that this troilite was partially fused and than transferred into the silicate melt pockets. The main open question is the overall SiO_2 budget, as there was no external Si source assuming that orthopyroxene was produced from, and equilibrated with olivine. The thermally induced breakdown of a hypothetical Si-rich, Ca- and P-bearing Mg-silicate could explain both symplectite formation and the emergence of residual keplerite droplets. However, no minerals with the acceptable composition were so far encountered in pallasites.

In contrast to pallasites, the origin of keplerite in the angrite meteorites (e.g., Keil et al. 1976; Crozaz and McKay 1990) is clearly related to the general crystallization pathways of these basaltic systems, which are reviewed in detail by Keil (2012). The variations in Mg/Fe ratio result in the emergence of an isomorphous series between keplerite and its Fe^{2+}-dominant analogue, matyhite (Hwang et al. 2019).

The formation of terrestrial keplerite in the pyrometamorphic paralavas of the Hatrurim Formation is related to the local geochemical "micro-environments" which produce the known mineral diversity of this unique rock complex. Mineral composition of keplerite-bearing paralava evidences that the primary source rocks for these assemblages were the paralavas related to the so-called "olive unit", whose likely protolith lithologies were the marls of the Taqiye Formation of Paleocene age (Burg et al. 1999). The origin of keplerite-bearing assemblages is related to the high-temperature alteration processes of primary paralavas of the olive unit, which were accompanied by brecciation of the rocks and the emergence of new generations of paralavas (Figure 4a). Accessory fluorapatite is a primary mineral in these paralavas, and keplerite was likely formed as a product of thermally induced defluorination of fluorapatite (Figure 4c d). Where the latter was stuffed with the inclusions of xenotime and monazite, it was transformed into keplerite having high *REE* contents.

The association of keplerite with merrillite, "*REE*-merrillite" and stanfieldite (Table 3) evidences that the temperature conditions governed the formation of these phosphate assemblages were similar to those encountered during formation of meteorites and Lunar rocks.

Keplerite position in the whitlockite group and the Na-number

The crystal structure of whitlockite and related minerals bear three 8-coordinated [AO_8] polyhedra, which in total account for 9 Ca atoms per $A_9BM(PO_3X)_4(PO_4)_3$ formula unit, that corresponds to almost 50 wt.% CaO in the chemical composition. Geochemical conditions leave a little chance for any element to compete with Ca for the domination in the [AO_8] polyhedra; the sole exception is strontiowhitlockite, where *A* = Sr (Britvin et al. 1991). As a consequence, the mineral diversity within the whitlockite group is produced by (1) the interplay between substitutions at the *B* and *M* sites, and (2) the attachment of acidic hydrogen(s) to $[PO_4]^{3-}$ tetrahedra to form hydrogen phosphate anion(s), $[HPO_4]^{2-} \equiv [PO_3OH]^{2-}$ (Table 1). Keplerite is related to its Na-counterpart, merrillite, by the heterovalent isomorphous substitution at the *B*-site of the crystal structure: $2Na^{+}$ (merrillite) → $Ca^{2+} + \square$ (keplerite) and thus represents a distinct species (Hatert and Burke 2008; Bosi et al. 2019). The introduction of a trivial name for keplerite highlights the chemical and genetic difference between this mineral and other whitlockite-group species (Table 1). There still a substantial disorder in the literature concerning whitlockite-group minerals, in particular – intermixing of the names *merrillite* [an *anhydrous* $Ca_9NaMg(PO_4)_7$] and *whitlockite* [*water*-containing $Ca_9Mg(PO_3OH)(PO_4)_6$] (e.g., Sha 2000; Ionov et al. 2006; Pasek 2015; Keil and McCoy 2018; Carrillo-Sánchez et al. 2020). Meanwhile, the difference between water-containing and anhydrous mineral looks not negligible but of paramount importance while dealing with the reconstructions of geochemical/cosmochemical processes (Pernet-Fisher et al. 2014). The names like "Ca-merrillite" appear to add even more confusion, as merrillite itself, $Ca_9NaMg(PO_4)_7$, is a Ca-dominant mineral

405 by definition, contrary to, e.g., strontiowhitlockite, $Sr_9Mg(PO_3OH)(PO_4)_6$ (Britvin et al. 1991).
406 However, the general name *merrillite* is convenient for the use as a subgroup (≡ structure type) root
407 name, like the commonly used root names *tourmaline*, *garnet*, *plagioclase*, etc. Because the
408 minerals related to the join merrillite–keplerite are ubiquitous in the extraterrestrial matter, it appears
409 to be convenient to quantify the role of Na in their composition (by analogy with, e.g., plagioclases).
410 For this purpose, we herein propose the introduction of the Na-number (like a common Mg-
411 number), formulated as 100×Na/(Na+Ca) in atomic amounts (Table 2). The merrillite end-member,
412 $Ca_9NaMg(PO_4)_7$, has thus the Na-number = 10 whereas keplerite, $Ca_9(Ca_{0.5}\square_{0.5})Mg(PO_4)_7$, has the
413 Na-number = 0.
414

415 **Implications**

416 The minerals belonging to the solid solutions merrillite–keplerite represent quite an important
417 reservoir of phosphate phosphorus in the different kinds of the Solar System objects, from chondritic
418 and achondritic meteorites, stony-irons and irons to the Lunar and Martian rocks. The discovery of
419 these minerals in the Earth's mantle xenoliths (Ionov et al. 2006) and in the pyrometamorphic
420 complex of the Hatrurim Formation opens new insights into their occurrence in the terrestrial rocks.
421 Their crystal structures favor the selective accumulation of rare earth elements and actinides, serving
422 these minerals as convenient targets for geological dating (Snape et al. 2016). The phase
423 transformations of merrillite-type minerals into the high-pressure γ-$Ca_3(PO_4)_2$ polymorph (tuite) are
424 the sensitive indicators of impact events experienced by the parent celestial bodies (Xie et al. 2002).
425 Therefore, revealing the new structural and genetic relationships between merrillite–keplerite
426 minerals and associated phases would add more knowledge towards understanding the processes of
427 the Solar System formation.
428

Acknowledgments

The authors are thankful to the curators of the Mining Museum, St. Petersburg Mining Institute, for providing meteorite samples. We are grateful to Associate Editor Fabrizio Nestola for the handling of the manuscript, and to the Technical Editor for the correction of crystallographic data. The authors are indebted to the reviewers, Pietro Vignola and Ferdinando Bosi, who made valuable suggestions that substantially enhanced the contents of the article. This research was supported by Russian Science Foundation, grant 18-17-00079 (the study of holotype, meteoritic keplerite), and by the National Science Centre (NCN) of Poland, grant no. 2016/23/B/ST10/00869 (the part related to terrestrial keplerite). We thank X-ray Diffraction Centre and "Geomodel" Resource Centre of St. Petersburg State University for instrumental and computational support.

References cited

Adcock, C.T., Hausrath, E.M., Forster, P.M., Tschauner, O., and Sefein, K.J. (2014) Synthesis and characterization of the Mars-relevant phosphate minerals Fe and Mg-whitlockite and merrillite and a possible mechanism that maintains charge balance during whitlockite to merrillite transformation. American Mineralogist, 99, 1221–1232.

Beck, S.D. (2011) Variations in recorded acoustic gunshot waveforms generated by small firearms. The Journal of the Acoustical Society of America, 129, 1748–1759.

Belik, A.A., Izumi, F., Stefanovich, S.Yu., Lazoryak, B.I., and Oikawa, K. (2003) Chemical and structural properties of a whitlockite-like phosphate,$Ca_9FeD(PO_4)_7$.Chemistry of Materials, 15, 1399–1400.

Boesenberg, J.S., Delaney, G.S., and Hewins, R.H.J. (2012) A petrological and chemical reexamination of Main Group pallasite formation.Geochimica et Cosmochimica Acta, 89, 134–158.

453 Bondar, Yu.V., and Perelygin, V.P. (2005) Fission-track analysis of meteorites: Dating of the
454 Marjalahti pallasite. Radiation Measurements, 40, 522–527.
455 Bosi, F., Hatert, F., Hålenius, U., Pasero, M., Miyawaki, R., and Mills, S,J, (2019) On the
456 application of the IMA-CNMNC dominant-valency rule to complex mineral compositions.
457 Mineralogical Magazine, 83, 627–632.
458 Britvin, S.N., Krivovichev, S.V., and Armbruster, T. (2016) Ferromerrillite, $Ca_9NaFe^{2+}(PO_4)_7$, a
459 new mineral from the Martian meteorites, and some insights into merrillite–tuite
460 transformation in shergottites. European Journal of Mineralogy, 28, 125–136.
461 Britvin, S.N., Krzhizhanovskaya, M.G., Bocharov, V.N., and Obolonskaya, E.V. (2020) Crystal
462 chemistry of stanfieldite, $Ca_7M_2Mg_9(PO_4)_{12}$ (M = Ca, Mg, Fe^{2+}), a structural base of
463 $Ca_3Mg_3(PO_4)_4$ phosphors. Crystals, 10, 464.
464 Britvin, S.N., Murashko, M.N., Vapnik,Ye., Polekhovsky, Yu.S., and Krivovichev, S.V. (2015)
465 Earth's phosphides in Levant and insights into the source of Archaean prebiotc phosphorus.
466 Scientific Reports, 5, 8355.
467 Britvin, S.N., Pakhomovskii, Ya.A., Bogdanova, A.N., and Skiba, V.I. (1991) Strontiowhitlockite,
468 $Sr_9Mg(PO_3OH)(PO_4)_6$, a new mineral species from the Kovdor deposit, Kola Peninsula,
469 U.S.S.R. Canadian Mineralogist, 29, 87–93.
470 Burg, A., Kolodny, Ye., and Lyakhovsky, V. (1999) Hatrurim - 2000: The "Mottled Zone" revisited,
471 forty years later. Israel Journal of Earth Sciences, 48, 209–223.
472 Buseck, P.R. (1977) Pallasite meteorites – mineralogy, petrology and geochemistry. Geochimica et
473 Cosmochimica Acta, 41, 711–740.
474 Buseck, P.R., and Holdsworth, E. (1977) Phosphate minerals in pallasite meteorites. Mineralogical
475 Magazine, 41, 91–102.

476 de Aza, P.N., Santos, C., Pazo, A., de Aza, S., Cuscó R., and Artús, L. (1997) Vibrational properties
477 of calcium phosphate compounds.1.Raman spectrum of β-Tricalcium Phosphate. Chemistry of
478 Materials, 9, 912–915.
479 Calvo, C., and Gopal, R. (1975) The crystal structure of whitlockite from the Palermo Quarry.
480 American Mineralogist, 60, 120–133.
481 Carrillo-Sánchez, J.D., Bones, D.L., Douglas, K.M., Flynn, G.J., Wirick, S., Fegley, B.Jr., Araki, T.,
482 Kaulich, B., and Plane, J.M.C. (2020) Injection of meteoric phosphorus into planetary
483 atmospheres. Planetary and Space Science, 187, 104926.
484 Cooper, M.A., Hawthorne, F.C., Abdu, Y.A., Ball, N.A., Ramik, R.A., and Tait, K.T. (2013)
485 Wopmayite, ideally $Ca_6Na_3Mn(PO_4)_3(PO_3OH)_4$, a new phosphate mineral from the Tanco
486 Mine, Bernic Lake, Manitoba: Description and crystal structure. Canadian Mineralogist, 51,
487 93–106.
488 Crozaz G., and McKay, G. (1990) Rare earth elements in Angra dos Reis and Lewis Cliff 86010,
489 two meteorites with similar but distinct magma evolutions. Earth and Planetary Science
490 Letters, 97, 369–381.
491 Dolomanov, O.V., Bourhis, L.J., Gildea, R.J., Howard, J.A., and Puschmann, H. (2009) OLEX2: a
492 complete structure solution, refinement and analysis program. Journal of Applied
493 Crystallography, 42, 339–341.
494 Dowty, E. (1977) Phosphate in Angra dos Reis: Structure and composition of the $Ca_3(PO_4)_2$
495 minerals. Earth and Planetary Science Letters, 35, 347–351.
496 El Goresy, A., Zinner, E., Pellas, P., and Caillet, C. (2005) A menagerie of graphite morphologies in
497 the Acapulco meteorite with diverse carbon and nitrogen isotopic signatures: implications for
498 the evolution history of acapulcoite meteorites. Geochimica et Cosmochimica Acta, 69, 4535–
499 4556.

Folco, L., D'Orazio, M., and Burroni, A. (2006) Frontier Mountain 93001: A coarse-grained, enstatite-augite-oligoclase-rich, igneous rock from the acapulcoite-lodranite parent asteroid. Meteoritics & Planetary Science, 41, 1183–1198.

Frondel, C. (1941) Whitlockite: a new calcium phosphate $Ca_3(PO_4)_2$. American Mineralogist, 26, 145–152.

Frondel, C. (1943) Mineralogy of the calcium phosphates in insular phosphate rock. American Mineralogist, 28, 215–232.

Fuchs, L.H. (1962) Occurrence of whitlockite in chondritic meteorites. Science, 137, 425–426.

Galuskin, E.V., Galuskina, I.O., Gfeller, F., Krüger, B., Kusz, J., Vapnik, Ye., Dulski, M., and Dzierżanowski, P. (2016): Silicocarnotite, $Ca_5[(SiO_4)(PO_4)](PO_4)$, new "old" mineral from the Negev Desert, Israel, and the ternesite–silicocarnotite solid solution: indicators of high-temperature alteration of pyrometamorphic rocks of the Hatrurim Complex, Southern Levant. European Journal of Mineralogy, 28, 105–123.

Galuskin, E.V., Krüger, B., Galuskina, I.O., Krüger, H., Vapnik, Ye., Wojdyla, J.A., and Murashko, M. (2018a) New mineral with modular structure derived from hatrurite from the pyrometamorphic rocks of the Hatrurim Complex: Ariegilatite, $BaCa_{12}(SiO_4)_4(PO_4)_2F_2O$, from Negev Desert, Israel. Minerals, 8, 19

Galuskin, E.V., Krüger, B., Galuskina, I.O., Krüger, H., Vapnik, Ye., Pauluhn, A., and Olieric, V. (2018b) Stracherite, $BaCa_6(SiO_4)_2[(PO_4)(CO_3)]F$, the first CO_3-bearing intercalated hexagonal antiperovskite from Negev Desert, Israel. American Mineralogist, 103, 1699–1706.

Galuskina, I.O., Vapnik, Ye., Lazic, B., Armbruster, T., Murashko, M., and Galuskin, E.V. (2014) Harmunite $CaFe_2O_4$: a new mineral from the Jabel Harmun, West Bank, Palestinian Autonomy, Israel. American Mineralogist, 99, 965–975.

Galuskina, I.O., Galuskin, E.V., and Vapnik, Y.A. (2016) Terrestrial merrillite. 2nd European Mineralogical Conference, Plinius, 42, 563 (abstr.).

525 Geller, Y.I., Burg, A., Halicz, L. and Kolodny, Y. (2012) System closure during the combustion
526 metamorphic ”Mottled Zone” event, Israel. Chemical Geology, 334, 25–36.
527 Gopal, R. and Calvo, C. (1972) Structural relationship of whitlockite and β-$Ca_3(PO_4)_2$. Nature
528 Physical Sciences, 237, 30–32.
529 Grady, M.M. (2000) Catalogue of Meteorites.Cambridge University Press, Cambridge, New York.
530 Gross, H. (1977) The mineralogy of the Hatrurim Formation, Israel.Geological Survey of Israel
531 Bulletin, 70, 1–80.
532 Goodrich, C.A., Kita, N.T., Sutton, S.R., Wirick, S., and Gross, J. (2017) The Miller Range 090340
533 and 090206 meteorites: Identification of new brachinite-like achondrites with implications for
534 the diversity and petrogenesis of the brachinite clan. Meteoritics & Planetary Science, 52, 949–
535 978.
536 Hatert, F., and Burke, E.A.J. (2008) The IMA–CNMNC dominant-constituent rule revisited and
537 extended. The Canadian Mineralogist, 46, 717–728.
538 Hughes, J.M., Jolliff, B.L., and Gunter, M.E. (2006) The atomic arrangement of merrillite from the
539 Fra Mauro Formation, Apollo 14 lunar mission: The first structure of merrillite from the
540 Moon. American Mineralogist, 91, 1547–1552.
541 Hughes, J.M., Jolliff, B.L., and Rakovan, J. (2008) The crystal chemistry of whitlockite and
542 merrillite and the dehydrogenation of whitlockite to merrillite. American Mineralogist, 93,
543 1300–1305.
544 Hwang, S.-L., Shen, P., Chu, H.-T., Yui, T.-F., Varela, M.E., and Iizuka, Y. (2019) New minerals
545 tsangpoite $Ca_5(PO_4)_2(SiO_4)$ and matyhite $Ca_9(Ca_{0.5}\square_{0.5})Fe(PO_4)_7$ from the D'Orbigny angrite.
546 Mineralogical Magazine, 83, 293–313.
547 Ionov, D.A., Hofmann, A.W., Merlet, C., Gurenko, A.A., Hellebrand, E., Montagnac, G., Gillet, P.,
548 and Prikhodko, V.S. (2006) Discovery of whitlockite in mantle xenoliths: Inferences for water-

549 and halogen-poor fluids and trace element residence in the terrestrial upper mantle. Earth and
550 Planetary Science Letters, 244, 201–217.
551 Jolliff, B.L., Freeman, J.J., and Wopenka, B. (1996) Structural comparison lunar, terrestrial, and
552 synthetic whitlockite using laser Raman microprobe spectroscopy. Lunar and Planetary
553 Science XXII, 613–614 (abstr.).
554 Jolliff, B.L., Hughes, J.M., Freeman, J.J., and Zeigler, R.A. (2006) Crystal chemistry of lunar
555 merrillite and comparison to other meteoritic and planetary suites of whitlockite and merrillite.
556 American Mineralogist, 91, 1583–1595.
557 Jones, R.H., McCubbin, F.M., Dreeland, L., Guan, Y.B., Burger, P.V., and Shearer, C.K. (2014)
558 Phosphate minerals in LL chondrites: A record of the action of fluids during metamorphism on
559 ordinary chondrite parent bodies. Geochimica et Cosmochimica Acta, 132, 120–140.
560 Jones, R.H., McCubbin, F.M., and Guan, Y. (2016) Phosphate minerals in the H group of ordinary
561 chondrites, and fluid activity recorded by apatite heterogeneity in the Zag H3-6 regolith
562 breccia. American Mineralogist, 101, 2451–2467.
563 Keil, K. (2012) Angrites, a small but diverse suite of ancient, silica-undersaturated volcanic-plutonic
564 mafic meteorites, and the history of their parent asteroid. Chemie der Erde – Geochemistry, 72,
565 191–218.
566 Keil, K., Prinz, M., Hlava, P.F., Gomes, C.B., Curvello, W.S., Wasserburg, G.J., Tera, F.,
567 Papanastassiou, D.A., Huneke, J.C., Murali, A.V., Ma, M.-S., Schmitt, R.A., Lugmair, G.W.,
568 Marti, K., Scheinin, N.B., Clayton, R.N. (1976) Progress by the consorts of Angra dos Reis
569 (The Adorables). Abstracts of Lunar and Planetary Science Conference, 7, 443–445.
570 Keil, K., and McCoy, T.J. (2018) Acapulcoite-lodranite meteorites: Ultramafic asteroidal partial
571 melt residues.Chemie der Erde – Geochemistry, 78, 153–203.
572 Kepler, I. (1611) Strena seu de nive sexangula. Godefridum Tampach, Francofurti ad Moenum.

573 Khoury, H.N. (2020) High- and low-temperature mineral phases from the pyrometamorphic rocks,
574 Jordan. Arabian Journal of Geosciences, 13, 734.
575 Kovyazina, S.A., Perelyaeva, L.A., Leonidova, O.N., Leonidov, I.A., and Ivanovskii, A.L. (2004)
576 High-temperature Raman spectroscopy and phase transformations in phosphates and vanadates
577 $Ca_{3-3x}Nd_{2x}(AO_4)_2$ (A = P, V; $0 \le x \le 0.14$). Crystallography Reports, 49, 211–214.
578 Krüger, B., Krüger, H., Galuskin, E.V., Galuskina, I.O., Vapnik, Ye., Olieric, V., and Pauluhn, A.
579 (2018) Aravaite, $Ba_2Ca_{18}(SiO_4)_6(PO_4)_3(CO_3)F_3O$: modular structure and disorder of a new
580 mineral with single and triple antiperovskite layers. Acta Crystallographica, B74, 492–501.
581 Krüger, B., Galuskin, E.V., Galuskina, I.O., Krüger, H., and Vapnik, Y. (2019) Kahlenbergite, IMA
582 2018-247. CNMNC Newsletter No. 49, Mineralogical Magazine, 83, 479–493.
583 Lewis, J. and Jones, R.H. (2016) Phosphate and feldspar mineralogy of equilibrated L chondrites:
584 The record of metasomatism during metamorphism in ordinary chondrite parent bodies.
585 Meteoritics & Planetary Science, 51, 1886–1913.
586 Mandarino, J.A. (1981) The Gladstone-Dale relationship.IV.The compatibility concept and its
587 application. Canadian Mineralogist, 19, 441–450.
588 McCubbin, F.M., and Jones, R.H. (2015) Extraterrestrial apatite: Planetary geochemistry to
589 astrobiology. Elements, 11, 183–188.
590 Merrill, G.P. (1915) On the monticellite-like mineral in meteorites, and on oldhamite as a meteoric
591 constituent. Proceedings of the National Academy of Sciences, 1, 302–308.
592 Moore, P.B. (1973) Bracelets and pinwheels: a topological-geometric approach to the calcium
593 orthosilicates and alkali sulfate structures. American Mineralogist, 58, 32–42.
594 Novikov, I., Vapnik, Ye., and Safonova, I. (2013) Mud volcano origin of the Mottled Zone,
595 Southern Levant. Geoscience Frontiers, 4, 597–619.
596 Oxford Diffraction (2018) CrysAlisPro 171.40. Oxford Diffraction Ltd, Abingdon, England.
597 Pasek, M. (2015) Phosphorus as a lunar volatile. Icarus, 255, 18–23.

598 Patzer, A., and McSween, H.Y. (2012) Ordinary (mesostasis) and not-so-ordinary (symplectites)
599 late-stage assemblages in howardites. Meteoritics & Planetary Science, 47, 1475–1490.
600 Pellas, P., Perron, C., Crozaz, G., Perelygin, V.P., and Stetsenko, S.G. (1983) Fission track age and
601 cooling rate of the Marjalahti pallasite. Earth and Planetary Science Letters, 64, 319–326.
602 Pernet-Fisher, J.F., Howarth, G.H., Liu, Y., Chen, Y., and Taylor, L.A. (2014) Estimating the lunar
603 mantle water budget from phosphates: Complications associated with silicate-liquid-
604 immiscibility. Geochimica et Cosmochimica Acta, 144, 326–341.
605 Righter, K., Arculus, R.J., Paslick, C., and Delano, J.W. (1990) Electrochemical measurements and
606 thermodynamic calculations of redox equilibria in pallasite meteorites – Implications for the
607 eucrite parent body. Geochimica et Cosmochimica Acta, 54, 1803–1815.
608 Schroeder, L.W., Dickens, B., and Brown, W.E. (1977) Crystallographic studies of the role of Mg as
609 a stabilizing impurity in beta-$Ca_3(PO_4)_2$.II.Refinement of Mg-containing beta-$Ca_3(PO_4)_2$.
610 Journal of Solid State Chemistry, 22, 253–262.
611 Sha, L.K. (2000) Whitlockite solubility in silicate melts: Some insights into lunar and planetary
612 evolution. Geochimica et Cosmochimica Acta, 64, 3217–3236.
613 Shearer, C.K., Burger, P.V., Papike, J.J., McCubbin, F.M., and Bell, A.S. (2015) Crystal chemistry
614 of merrillite from Martian meteorites: Mineralogical recorders of magmatic processes and
615 planetary differentiation. Meteoritics & Planetary Science, 50, 649–673.
616 Sheldrick, G.M. (2015) Crystal structure refinement with *SHELXL*. Acta Crystallographica, C71, 3–
617 8.
618 Snape, J.F., Nemchin, A.A., Grange, M.L., Bellucci, J.J., Thiessen, F., and Whitehouse, M.J. (2016)
619 Phosphate ages in Apollo 14 breccias: Resolving multiple impact events with high precision
620 U–Pb SIMS analyses. Geochimica et Cosmochimica Acta, 174, 13–29.
621 Sokol, E.V., Kokh, S.N., Sharygin, V.V., Danilovsky, V.A., Seryotkin, Yu.V., Liferovich, R.,
622 Deviatiiarova, A.S., Nigmatulina, E.N., and Karmanov, N.S. (2019) Mineralogical diversity of

Ca_2SiO_4-bearing combustion metamorphic rocks in the Hatrurim Basin: implications for storage and partitioning of elements in oil shale clinkering. Minerals, 9, 465.

Uhlig, H.H. (1955) Contribution of metallurgy to the origin of meteorites Part II – The significance of Neumann bands in meteorites. Geochimica et Cosmochimica Acta, 7, 39–42.

Van Schmus, W.R., and Ribbe, P.H. (1969). Composition of phosphate minerals in ordinary chondrites. Geochimica et Cosmochimica Acta, 33, 637–640.

Vapnik, Ye., Sharygin, V.V., Sokol, E.V., and Shagam, R. (2007) Paralavas in a combustion metamorphic complex: Hatrurim Basin, Israel. The Geological Society of America, Reviews in Engineering Geology, 18, 133–153.

Wang, L., and Nancollas, G.H. (2008) Calcium orthophosphates: crystallization and dissolution. Chemical Reviews, 108, 4628–4669.

Ward, D., Bischoff, A., Roszjar, J., Berndt, J., and Whitehouse, M.J. (2017) Trace element inventory of meteoritic Ca-phosphates. American Mineralogist, 102, 1856–1880.

Witzke, T., Phillips, B.L., Woerner, W., Countinho, J.M.V., Färber, G., and Contreira Filho, R.R. (2015) Hedegaardite, IMA 2014-069. CNMNC Newsletter No.23, Mineralogical Magazine, 79, 51–58.

Xie, X., Minitti, M.E., Chen, M., Mao, H.K., Wang, D., Shu, J., and Fei, Y. (2002) Natural high-pressure polymorph of merrillite in the shock vein of the Suizhou meteorite. Geochimica et Cosmochimica Acta, 66, 2439–2444.

Xie, X., Yang, H., Gu, X., and Downs, R.T. (2015) Chemical composition and crystal structure of merrillite from the Suizhou meteorite. American Mineralogist, 100, 2753–2756.

645 **List of figure captions**

646

647 **Figure 1.** Neumann bands (shock-induced deformation twins) in the α-(Fe,Ni) metal matrix of the
648 Marjalahti pallasite. Polished section after nital etching. Photomicrograph in reflected light.

649

650 **Figure 2.** Keplerite-bearing assemblages in the Marjalahti pallasite. (a) Troilite-orthopyroxene
651 symplectites with two keplerite inclusions along the contact of olivine and α-(Fe,Ni) metal. The
652 Neumann bands penetrate the metal and abut against troilite. Reflected light. (b) Detail of the same
653 fragment. Note a porous microgranular troilite texture at the contact with symplectite. Reflected
654 light. (c) Detailed view of two keplerite inclusions depicted in (a). False color EDX map in
655 characteristic X-rays of respective elements. (d) SEM BSE image of keplerite inclusion embedded
656 in olivine. Abbreviations: Kpl, keplerite; Tr, troilite, Ol, olivine; Opx, orthopyroxene. The keplerite
657 grain marked as Kpl Str was used for X-ray structure determination.

658

659 **Figure 3.** Keplerite-bearing pyrometamorphic paralavas of the Hatrurim Basin, Negev desert, Israel.
660 (a) The outcrop of the paralava on the hill slope. (b) A close view of the paralava.

661

662 **Figure 4.** Keplerite-bearing assemblages in the paralava of the Hatrurim Basin. (a) Breccia-like rock
663 composed of grey fragments with red thin rims, cemented by green-yellow fragments and white
664 veinlets of secondary minerals. The fragments depicted in Figure 4c and 4b are shown in frames. (b)
665 The hematite-colored rim of grey breccia fragment. (c) Keplerite aggregates in the fine-grained
666 diopside paralava. A fragment magnified in Figure 4d is shown in frame. (d) A grain of keplerite
667 intergrown with fluorapatite. (e) Stanfieldite and *REE*-bearing keplerite in fluorapatite. (f) Xenotime
668 inclusions in fluorapatite. Mgh, maghemite; Di, diopside; Psb, pseudobrookite; Ap, fluorapatite;
669 Kpl, keplerite; Hm, hematite; Zlt, zeolites; Stf, stanfieldite; Wol, wollastonite; Xnt, xenotime-(Y).

670

671 **Figure 5.** The arrangement of species-defining [MO_6] octahedra (red) and [BO_6] polyhedra (green)
672 in the crystal structure of keplerite. Yellow: [PO_4] tetrahedra. The [AO_8] polyhedra are hidden for
673 clarity. A slice along the plane parallel to (0001).

674

675 **Figure 6.** *B*-site environment in the structure of keplerite, $Ca_9Ca_{1/2}Mg(PO_4)_7$ (this work) and
676 whitlockite-type $Ca_9FeD(PO_4)_7$ (Belik et al. 2003). (a) Keplerite (merrillite type): the *B* site is half-
677 occupied by Ca^{2+}, and the hydrogen-free tetrahedron [$P(1)O_4$] shares a common face with the apex-
678 truncated trigonal pyramid [BO_6]. (2) $Ca_9FeD(PO_4)_7$: the *B* site is devoid of cations but occupied by
679 a P–O pair of an inverted [$P(1')O_4$] tetrahedron. The apexes of four [PO_4] tetrahedra are tied up by
680 the triply split proton (deuteron) (blue) via the system of hydrogen bonds (dashed lines).

681

682 **Figure 7.** Raman spectra of (a) keplerite (the Marjalahti pallasite), (b) merrillite (the Brahin
683 pallasite), and (c) ferromerrillite (the Los Angeles shergottite). The spectra (b) and (c) are shifted
684 along the *x*-axis with the relative offset of 100 cm^{-1}.

685

686 **Figure 8.** Detailed view of the Raman bands related to ν_1 (symmetric stretching) vibrations of [PO_4]
687 tetrahedra. (a) Keplerite (the Marjalahti pallasite), with the band deconvolution curves; (b) merrillite
688 (the Brahin pallasite); and (c) ferromerrillite (the Los Angeles shergottite). Note the visually
689 resolved shoulders at 950 and 958 cm^{-1} in the spectrum of keplerite.

690 **Tables**

691
692 **Table 1.** Whitlockite-group minerals approved by CNMNC IMA [a]
693

Mineral [b]	Ideal formula	Species-defining constituents			
Anhydrous members		A	B	M	X
Merrillite [2]	$Ca_9NaMg(PO_4)_7$	Ca	Na	Mg	O
Keplerite [1]	$Ca_9(Ca_{0.5}\square_{0.5})Mg(PO_4)_7$	Ca	$Ca_{0.5}\square_{0.5}$	Mg	O
Ferromerrillite [3]	$Ca_9NaFe^{2+}(PO_4)_7$	Ca	Na	Fe^{2+}	O
Matyhite [4]	$Ca_9(Ca_{0.5}\square_{0.5})Fe^{2+}(PO_4)_7$	Ca	$Ca_{0.5}\square_{0.5}$	Fe^{2+}	O
Hydrogen-bearing members					
Whitlockite [5]	$Ca_9Mg(PO_3OH)(PO_4)_6$	Ca	$\square$	Mg	OH
Strontiowhitlockite [6]	$Sr_9Mg(PO_3OH)(PO_4)_6$	Sr	$\square$	Mg	OH
Wopmayite [7]	$Ca_6Na_3\square Mn^{2+}(PO_4)_3(PO_3OH)_4$	Ca	$\square$	Mn^{2+}	OH
Hedegaardite [8] [c]	$(Ca,Na)_9(Ca,Na)Mg(PO_3OH)(PO_4)_6$				

694
695 [a] Commission on New Minerals, Nomenclature and Classification of the International Mineralogical
696 Association. [b] References: [1] this work; [2] Xie et al. (2015); [3] Britvin et al. (2016); [4] Hwang et
697 al. (2019); [5] Calvo and Gopal (1975); [6] Britvin et al. (1991); [7] Cooper et al. (2013); [8] Witzke
698 et al. (2015). [c] Crystal structure of hedegaardite was not published.
699
700
701

Table 2. Chemical composition of meteoritic keplerite

Meteorite	Marjalahti		Angra dos Reis	Ahumada	Imilac	Somervell County	LEW 86010
Group	Pallasite		Angrite	Pallasite	Pallasite	Pallasite	Angrite
Reference [a]	[1]	[2]	[3]	[2]	[2]	[2]	[4]
				Wt.% [c]			
Na_2O	–	–	0.68	0.10	0.52	0.68	0.4
CaO	48.87	48.8	49.4	49.1	50.2	48.7	50.7
MgO	3.90	4.52	2.82	3.32	3.62	3.76	2.68
FeO	1.33	0.88	1.29	1.85	0.36	0.50	1.62
P_2O_5	46.24	45.2	45.1	45.6	45.9	46.8	44.6
SiO_2	–	–	0.67	0.32	–	0.08	0.68
Total	100.34	99.40	99.96	100.29	100.60	100.52	100.7
				Formula amounts (O = 28 *apfu*)			
Na	–	–	0.24	0.03	0.18	0.23	0.14
Ca	9.33	9.42	9.52	9.42	9.58	9.24	9.76
Σ(Ca,Na)	9.33	9.42	9.76	9.45	9.76	9.48	9.90
Mg	1.04	1.21	0.76	0.89	0.96	0.99	0.72
Fe^{2+}	0.20	0.13	0.19	0.28	0.05	0.07	0.24
Σ(Mg,Fe)	1.24	1.34	0.95	1.17	1.01	1.06	0.96
P	6.97	6.89	6.87	6.91	6.92	7.02	6.79
Si	–	–	0.12	0.06	–	0.01	0.12
Σ(P,Si)	6.97	6.89	6.99	6.97	6.92	7.03	6.91
Mg-number	84	90	80	76	94	93	75
Na-number	0	0	2.4	0.4	1.8	2.5	1.4

[a] References: [1] This work, holotype specimen; [2] Buseck and Holdsworth (1977); [3] Keil et al. (1976); [4] Crozaz and McKay (1990). [b] Contains 0.03 wt.% K_2O and 0.08 wt.% MnO (0.01 K and Mn *apfu*). [c] The dash means below detection limit.

Table 3. Chemical composition (wt.%) of keplerite and associated phosphates from the pyrometamorphic hornfels of the Hatrurim Basin

Phase number [a]	1	2	3	4	5	6
No. of points	3	1	10	4	2	6
CaO	48.39	46.64	45.61	42.22	23.20	54.66
SrO	– [b]	–	0.19	–	0.32	–
BaO	–	–	–	–	0.15	–
Na_2O	0.86	0.68	2.72	–	0.09	–
K_2O	–	–	0.12	–	–	–
MgO	3.73	3.72	3.50	3.50	23.67	0.56
MnO	–	–	–	–	0.13	0.06
FeO	–	0.65	0.15	0.35	3.11	0.20
Al_2O_3	–	–	–	0.05	–	–
Y_2O_3	–	0.76	0.43	3.75	–	–
La_2O_3	–	0.53	0.22	1.97	–	–
Ce_2O_3	–	0.27	–	1.27	–	–
Pr_2O_3	–	–	–	0.40	–	–
Nd_2O_3	–	0.43	0.24	1.93	–	–
Sm_2O_3	–	–	0.00	0.30	–	–
P_2O_5	45.85	45.25	45.12	43.54	49.52	42.04
V_2O_5	–	0.19	–	–	0.09	0.08
SiO_2	–	0.12	0.07	0.21	–	0.09
SO_3	–	0.19	0.24	0.30	0.26	0.07
F	tr [b]	tr	tr	tr	tr	3.82
$–O=F_2$						1.62
Total	98.83	99.43	98.61	98.79	100.54	99.96

[a] 1 – isolated keplerite grain; 2 – keplerite intergrown with fluorapatite (Figure 3d); 3 – merrilite; 4 – "*REE*-merrilite", 5 – stanfieldite; 6 – fluorapatite from the intergrowth with keplerite (Figure 3d). [b] The dash means below detection limit; tr – traces.

1: $Ca_{9.00}(Ca_{0.35}Na_{0.30})Mg_{1.00}(PO_4)_7$

2: $(Ca_{8.74}REE_{0.16}Mg_{0.10})_{9.00}(Ca_{0.30}Na_{0.24})_{0.54}(Mg_{0.90}Fe^{2+}_{0.10})_{1.00}[(PO_4)_{6.93}(SO_4)_{0.03}(SiO_4)_{0.02}(VO_4)_{0.02}]_7$

3: $(Ca_{8.87}REE_{0.07}Na_{0.04}Sr_{0.02})_{9.00}(Na_{0.92}K_{0.03})_{0.95}(Mg_{0.95}Ca_{0.03}Fe^{2+}_{0.02})_{1.00}[(PO_4)_{6.96}(SO_4)_{0.03}(SiO_4)_{0.01}]_7$

4: $(Ca_{8.18}REE_{0.78}Mg_{0.04})_{9.00}Ca_{0.11}(Mg_{0.94}Fe^{3+}_{0.05}Al_{0.01})_{1.00}[(PO_4)_{6.92}(SO_4)_{0.04}(SiO_4)_{0.04}]_7$

5: $(Ca_{6.88}Na_{0.05}Sr_{0.05}Ba_{0.02})_{7.00}(Mg_{1.04}Fe^{2+}_{0.74}Ca_{0.19}Mn^{2+}_{0.03})_{2.00}Mg_{9.00}[(PO_4)_{11.93}(SO_4)_{0.05}(VO_4)_{0.02})_{12}$

6: $(Ca_{4.91}Mg_{0.07}Fe^{2+}_{0.02})_{5.00}[(PO_4)_{2.98}(SiO_4)_{0.01}(SO_4)_{0.01}]_3F_{1.01}$

726 **Table 4.** Site populations and bond lengths for the *M* and *B* sites of keplerite and merrillite
727

Meteorite	Marjalahti	Angra dos Reis	Suizhou	Brahin
Mineral [a]	Keplerite [1]	Keplerite [2]	Merrillite [3]	Merrillite [4]
d(*M*—O6) (Å)	2.065(6)	2.078	2.070(2)	2.069(3)
d(*M*—O9) (Å)	2.093(6)	2.116	2.089(2)	2.091(3)
Mean *d*(*M*—O) (Å)	2.079	2.097	2.080	2.080
Site population (structure)	$Mg_{1.00}$ [b]	$Mg_{0.78}Fe_{0.22}$	$Mg_{0.95}Fe_{0.05}$	$Mg_{1.00}$ [b]
Site population (EMPA)	$Mg_{1.04}$	$Mg_{0.76}Fe_{0.19}$	$Mg_{0.95}Fe_{0.06}$	$Mg_{0.98}Fe_{0.01}$
d(*B*—O2) (Å)	2.790(9)	2.838	2.839(3)	2.848(5)
d(*B*—O3) (Å)	2.442(7)	2.442	2.411(2)	2.418(3)
Mean *d*(*X*—O) (Å)	2.616	2.640	2.625	2.633
Site population (structure)	$Ca_{0.33}Fe_{0.20}$ [c]	$Ca_{0.55(1)}$	$Na_{1.00}$ [d]	$Na_{1.00}$ [d]
Site scattering factor (*e*)	9.90 [e]	11.00 [e]	11.00 [d]	11.00 [d]
Site population (EMPA)	$Ca_{0.33}Fe_{0.20}$	$Ca_{0.52}Na_{0.24}$	$Na_{0.98}$	$Na_{1.00}$
Mean *Z* (EMPA) (*e*)	11.80	13.04	10.78	11.00

728
729 [a] References: [1] This work, holotype specimen; [2] Dowty (1977); [3] Xie et al. (2015); [4] Britvin
730 et al. (2016). [b] Refined Fe content lies within 2σ error. [c] Site population was fixed according to
731 EMPA results. [d] Not refined. [e] Freely refined electron density assuming Ca X-ray scattering curve.
732
733

734
735 **Table 5.** Frequencies of (PO_4) vibration modes (cm^{-1}) in the Raman spectra of keplerite,
736 merrillite and ferromerrillite
737

Mineral	Keplerite	Merrillite	Ferromerrillite
Meteorite	Marjalahti	Brahin	Los Angeles
Assignment [a]			
ν_2 (δ_s)	407	409	403
	442	446	445
ν_4 (δ_{as})	551	551	548
		593	591
	601	603	606
	622	618	620
		756	752
ν_1 (ν_s)	950 [b]		
	954	957	954
	958 [b]		
	971	973	970
ν_3 (ν_{as})	1016	1015	1012
	1078	1080	1080

738
739 [a] Band assignments according to de Aza et al. (1997); Kovyazina et al. (2004). [b] Only visually
740 resolved shoulders are listed (see Figure 7).
741
742

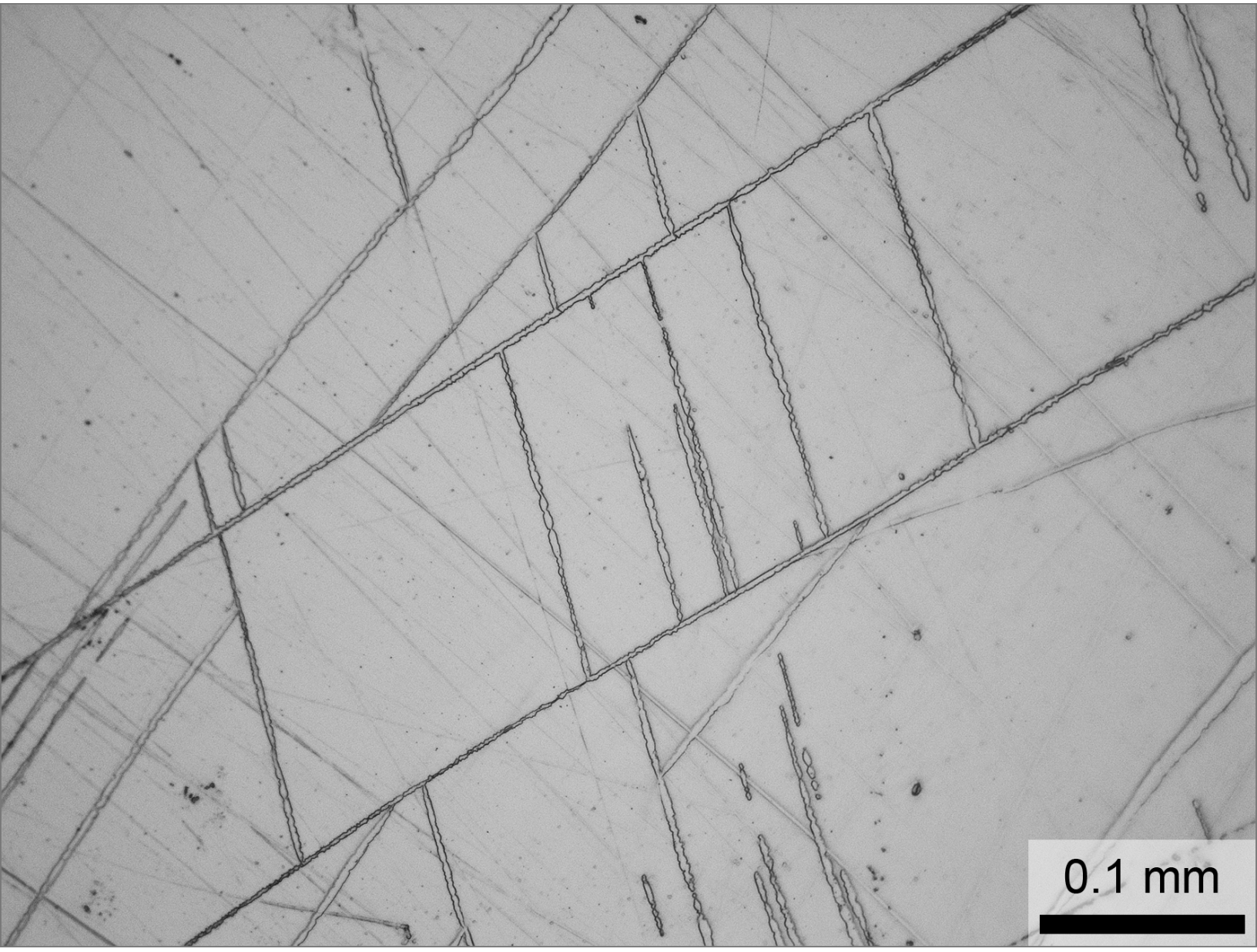
0.1 mm

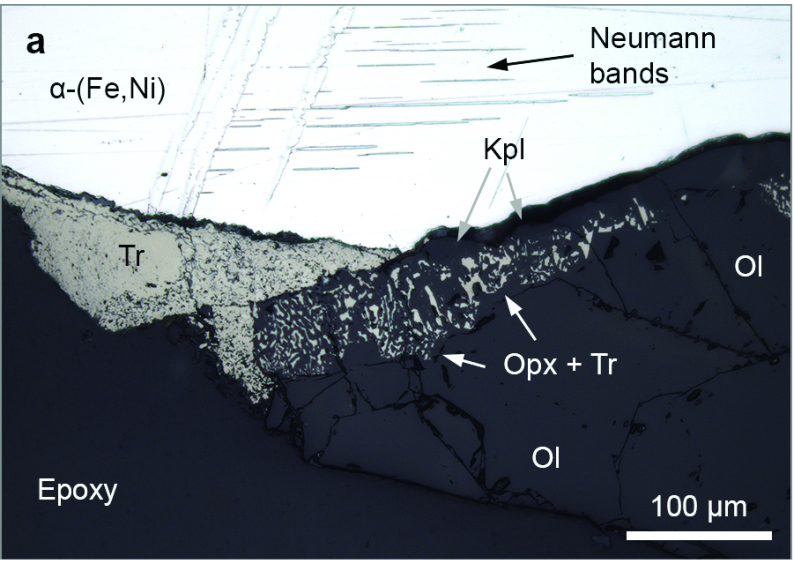
a
α-(Fe,Ni)
Neumann bands
Kpl
Tr
Ol
Opx + Tr
Ol
Epoxy
100 µm

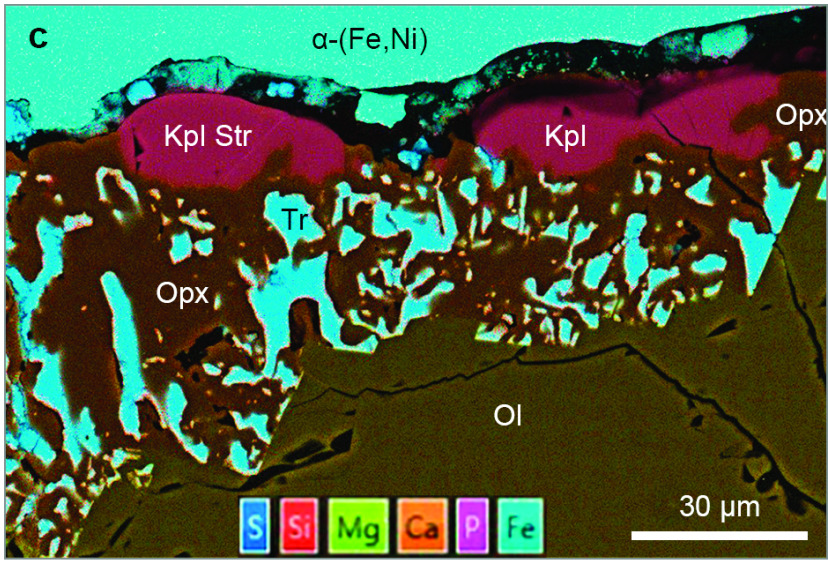
c
α-(Fe,Ni)
Kpl Str
Kpl
Opx
Tr
Opx
Ol
S
Si
Mg
Ca
P
Fe
30 µm

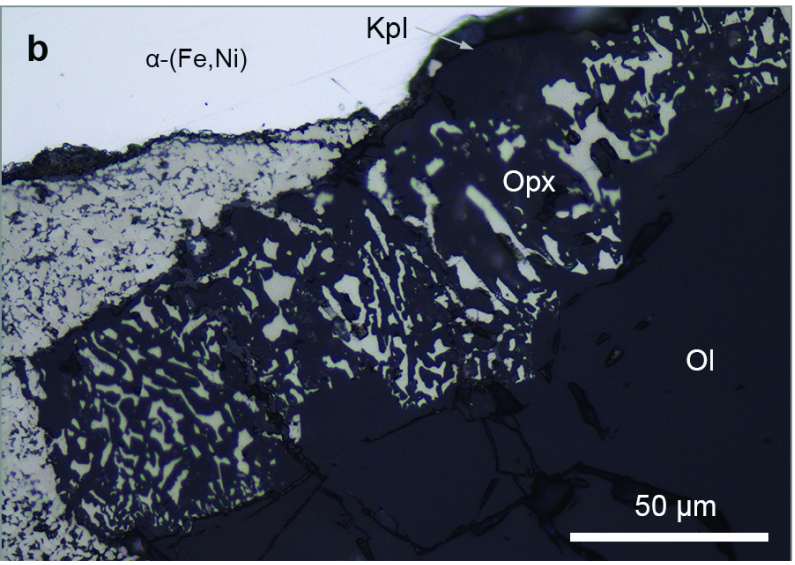
b
α-(Fe,Ni)
Kpl
Opx
Ol
50 µm

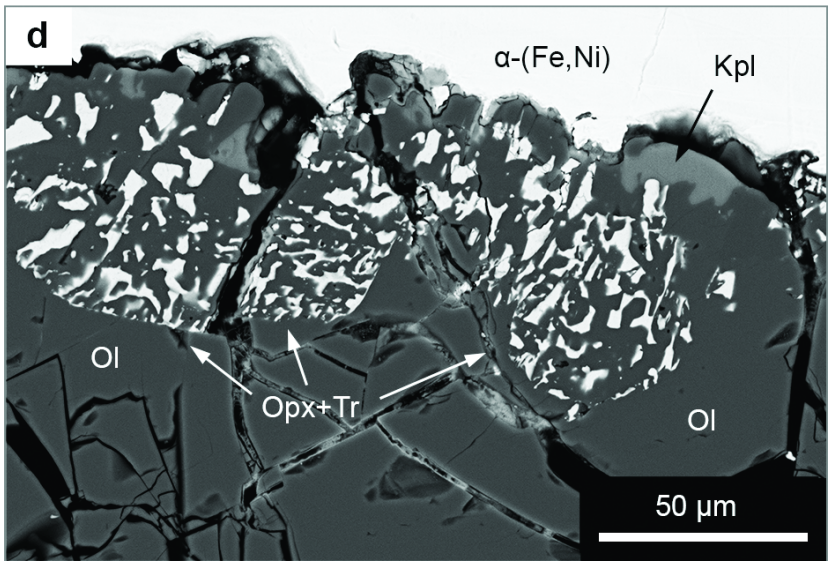
d
α-(Fe,Ni)
Kpl
Ol
Opx+Tr
Ol
50 µm


a


b

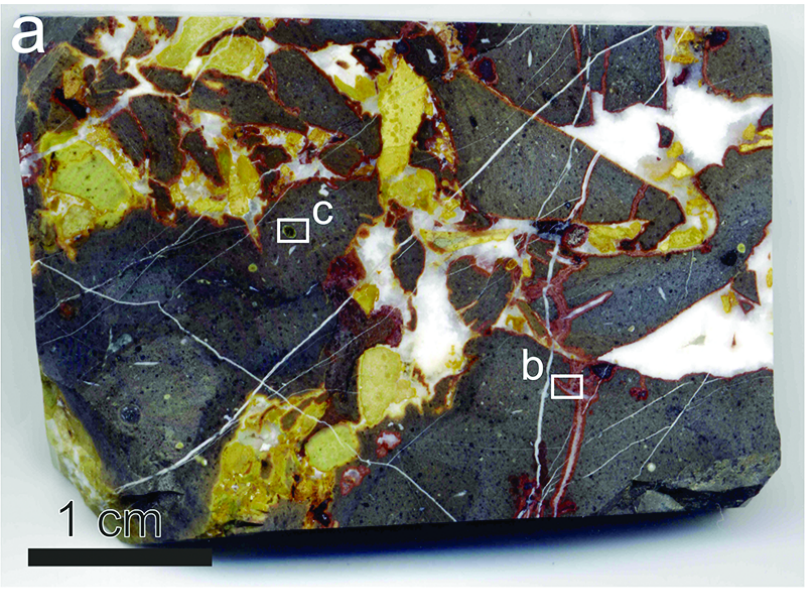
a
c
b
1 cm

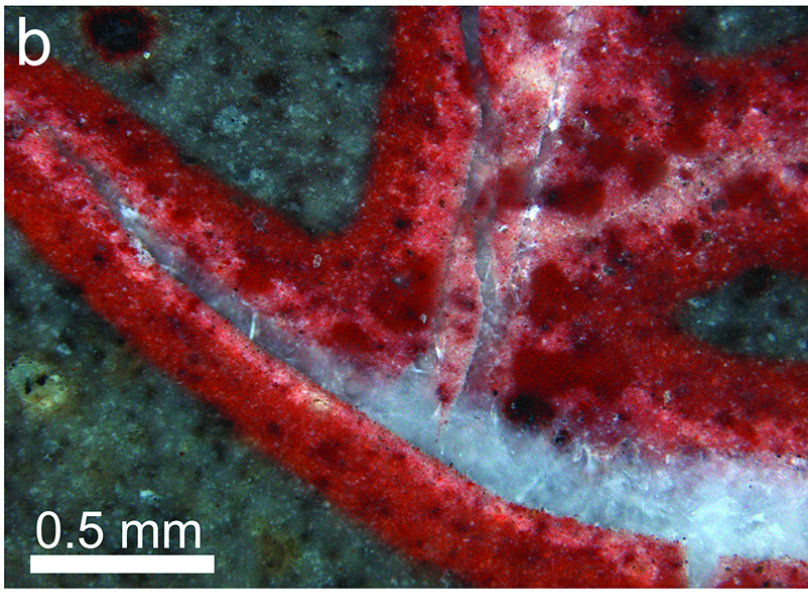
b
0.5 mm

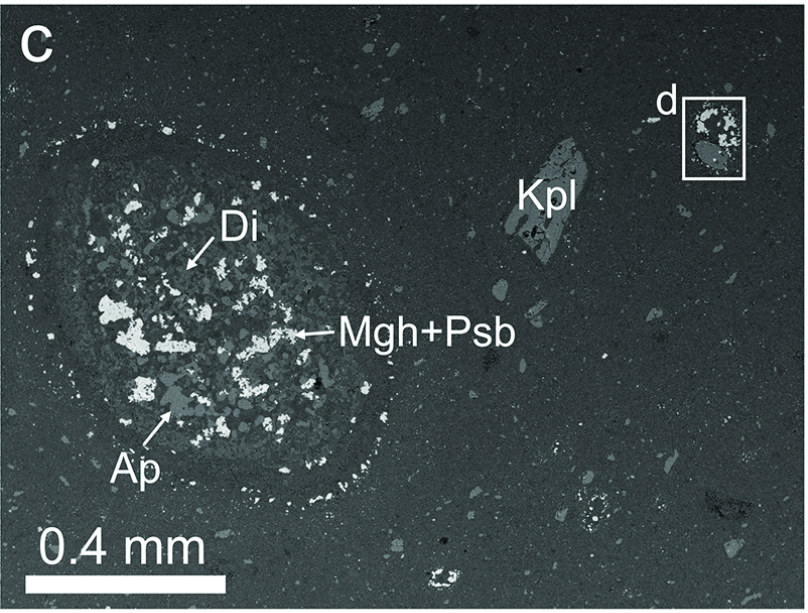
c
d
Kpl
Di
Mgh+Psb
Ap
0.4 mm

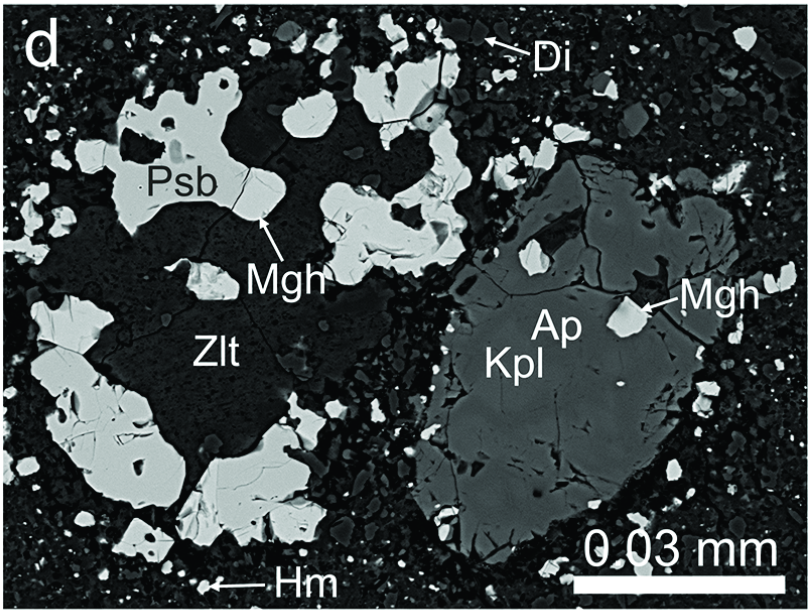
d
Di
Psb
Mgh
Mgh
Ap
Zlt
Kpl
0.03 mm
Hm

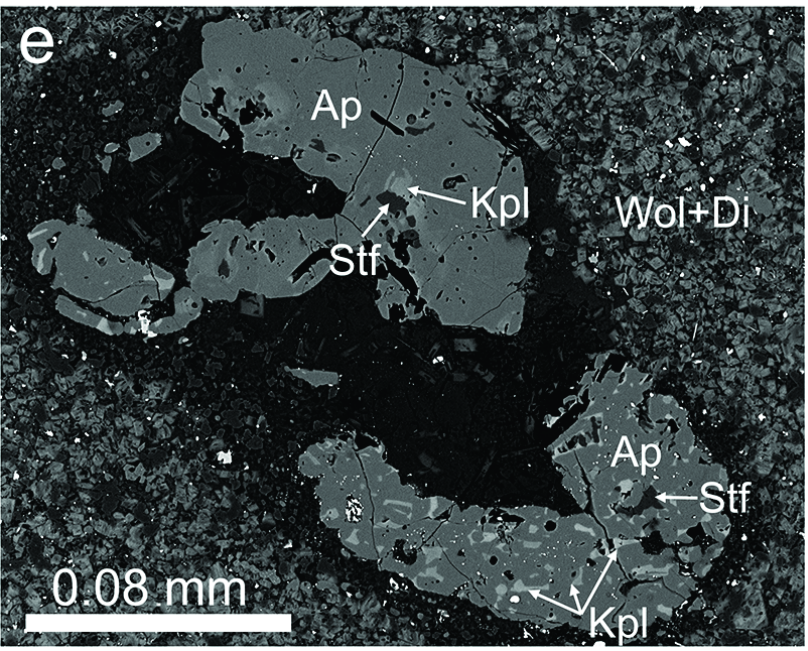
e
Ap
Kpl
Wol+Di
Stf
Ap
Stf
0.08 mm
Kpl

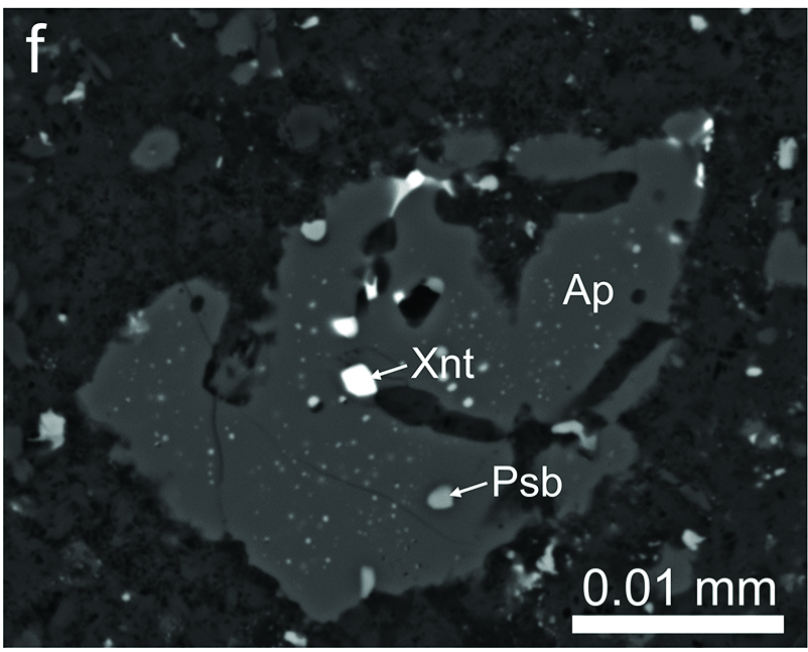
f
Ap
Xnt
Psb
0.01 mm

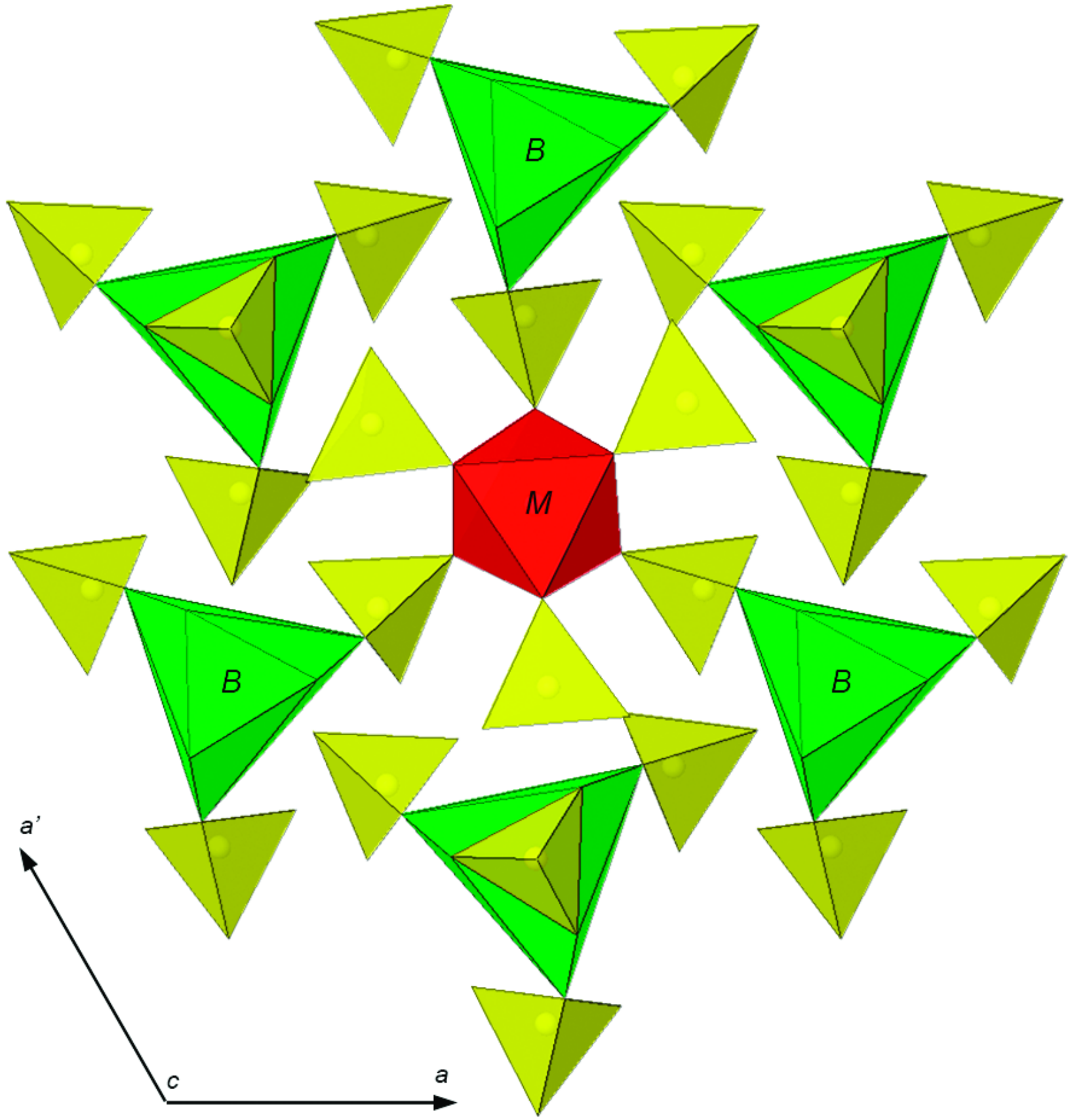
B
M
B
B
a'
c
a

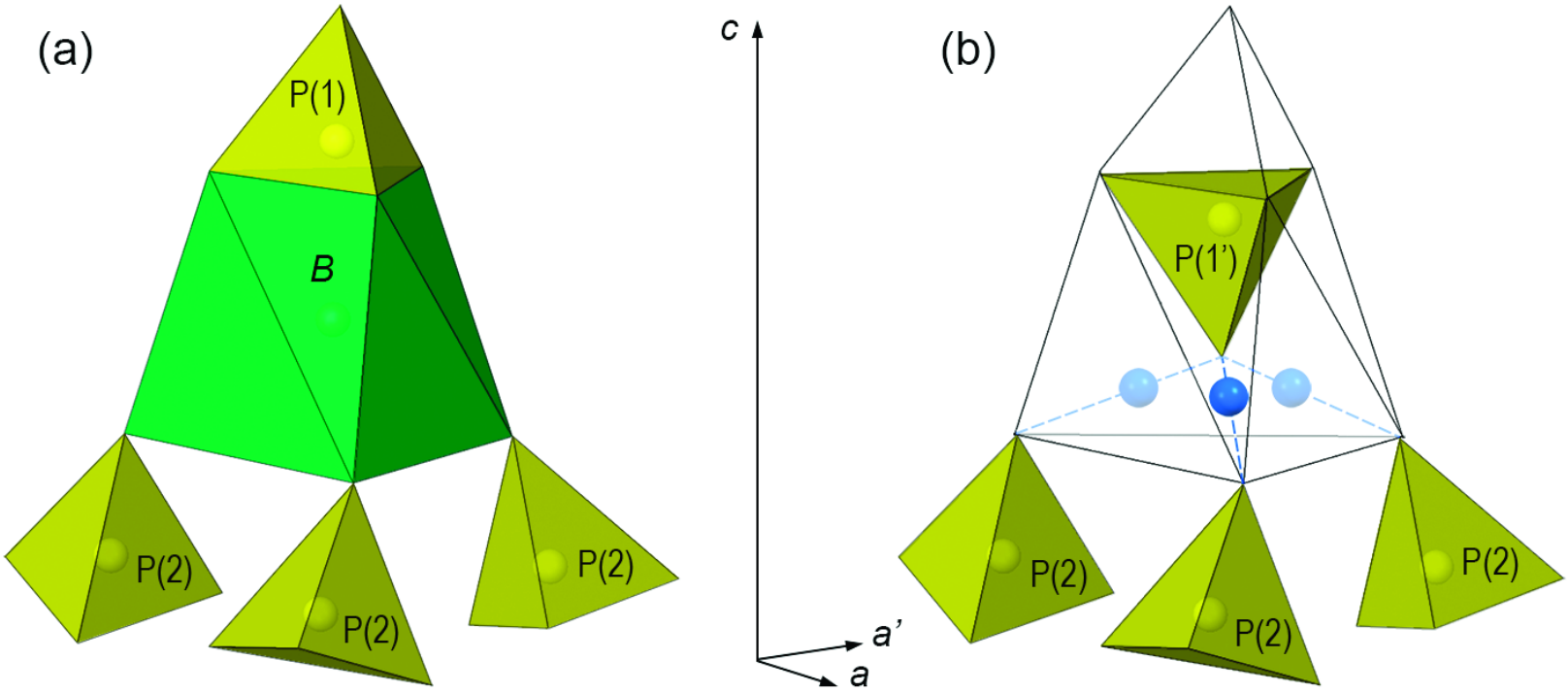
(a)
P(1)
B
P(2)
P(2)
P(2)
c
a'
a
(b)
P(1')
P(2)
P(2)
P(2)

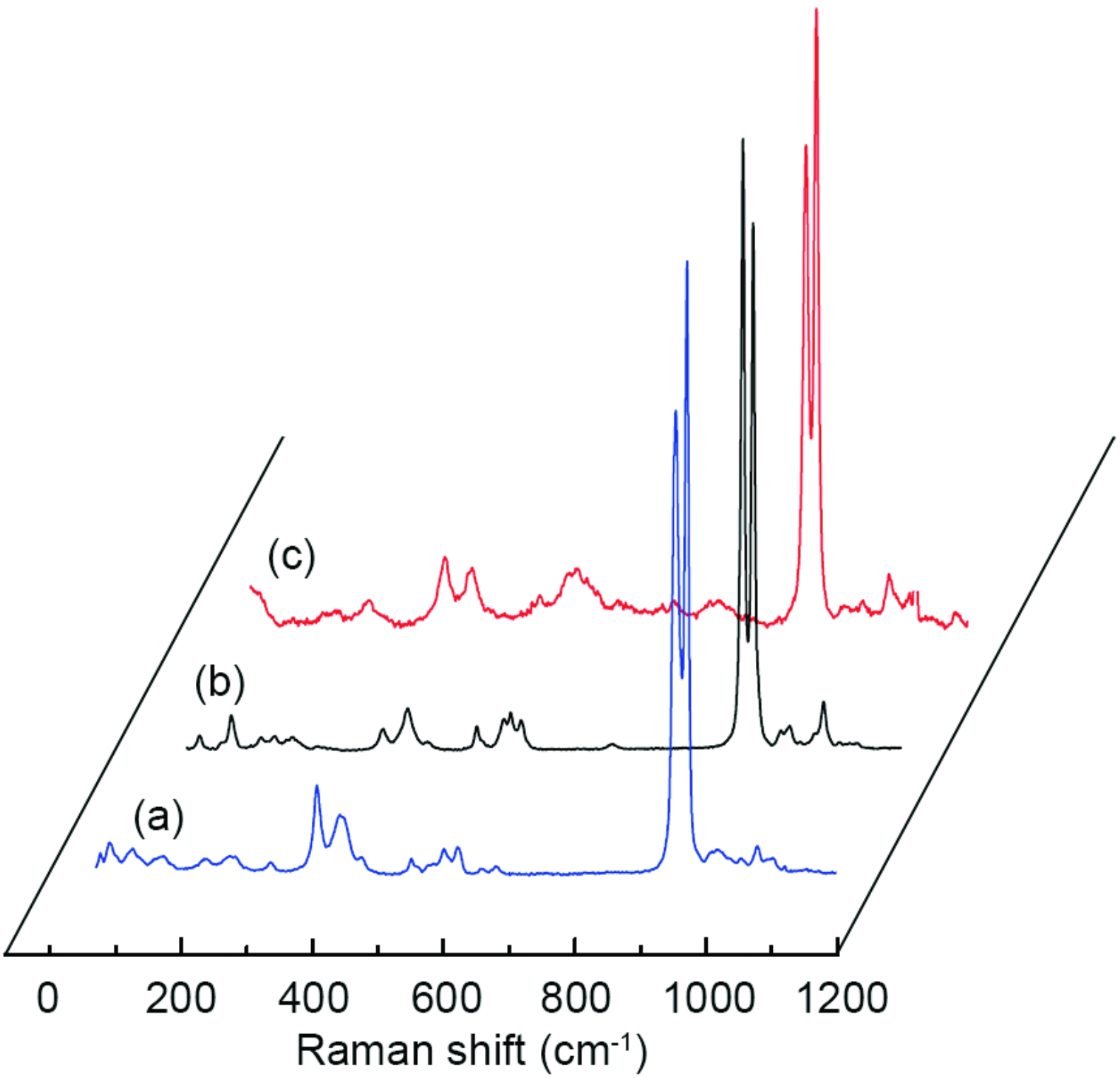
(c)
(b)
(a)
0
200
400
600
800
1000
1200
Raman shift (cm-1)

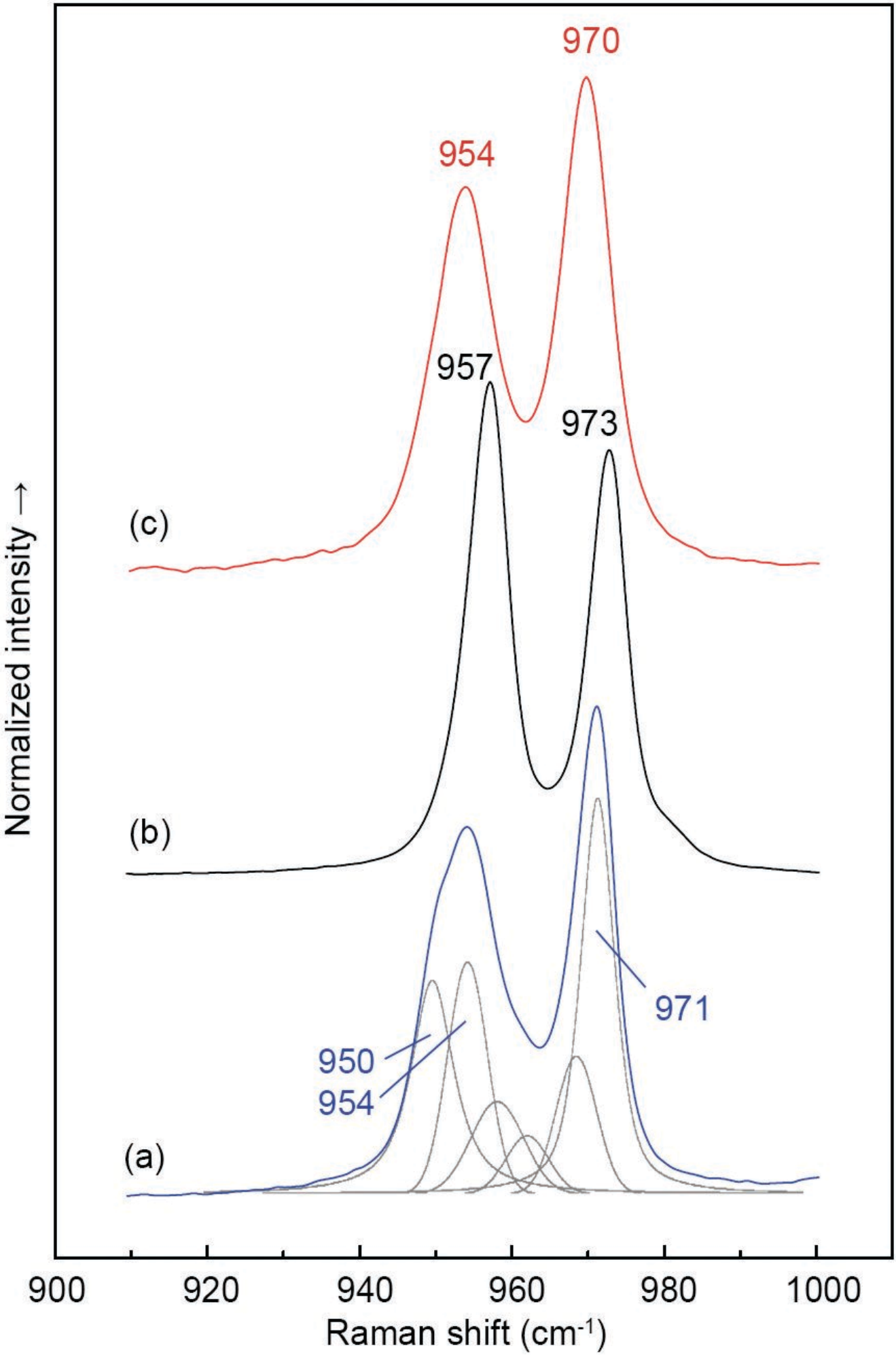
970
954
957
973
(c)
(b)
(a)
971
950
954
Normalized intensity →
900
920
940
960
980
1000
Raman shift (cm-1)